Journal of Medicinal Chemistry

ARTICLE

pubs.acs.org/jmc

In Vitro Cellular Uptake and Dimerization of Signal Transducer and Activator of Transcription-3 (STAT3) Identify the Photosensitizing and Imaging-Potential of Isomeric Photosensitizers Derived from Chlorophyll-*a* and Bacteriochlorophyll-*a*

Avinash Srivatsan,[†,#] Yanfang Wang,[†] Penny Joshi,[†] Munawwar Sajjad,[‡] Yihui Chen,[†] Chao Liu,[†] Krishnakumar Thankppan,[§] Joseph R. Missert,[†] Erin Tracy,[∥] Janet Morgan,[⊥] Nestor Rigual,[§] Heinz Baumann,[*,∥] and Ravindra K. Pandey[*,†,#]

Departments of [†]Cell Stress Biology/PDT Center, [§]Head and Neck/Plastic Surgery, [∥]Molecular and Cellular Biology, [⊥]Dermatology, and [#]Molecular Pharmacology and Cancer Therapeutics, Roswell Park Cancer Institute, Buffalo, New York 14263, United States

[‡]Department of Nuclear Medicine, SUNY, Buffalo, New York 14221

Supporting Information

ABSTRACT: Among the photosensitizers investigated, both ring-D and ring-B reduced chlorins containing the *m*-iodobenzyloxyethyl group at position-3 and a carboxylic acid functionality at position-17[2] showed the highest uptake by tumor cells and light-dependent photoreaction that correlated with maximal tumor-imaging [positron emission tomography (PET) and fluorescence] and long-term photodynamic therapy (PDT) efficacy in BALB/c mice bearing Colon26 tumors. However, among the ring-D reduced compounds, the isomer containing the 1′-*m*-iobenzyloxyethyl group at position-3 was more effective than the corresponding 8-(1′-*m*-iodobenzyloxyethyl) derivative. All photosensitizers showed maximum uptake by tumor tissue 24 h after injection, and the tumors exposed with light at low fluence and fluence rates (128 J/cm^2, 14 mW/cm^2) produced significantly enhanced tumor eradication than those exposed at higher fluence and fluence rate (135 J/cm^2, 75 mW/cm^2). Interestingly, dose-dependent cellular uptake of the compounds and light-dependent STAT3 dimerization have emerged as sensitive rapid indicators for PDT efficacy in vitro and in vivo and could be used as *in vitro/in vivo* biomarkers for evaluating and optimizing the in vivo treatment parameters of the existing and new PDT candidates.

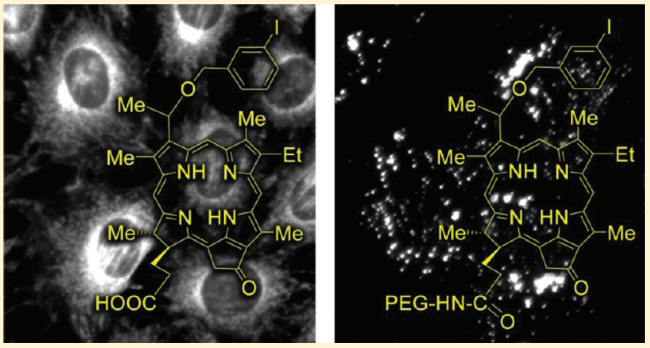

INTRODUCTION

Molecular imaging can be used for early detection and localization of lesions and for "real time" monitoring of the efficacy of therapeutic treatments.[1−3] In recent years, PET technology has been included in drug development, and it has contributed to the understanding of drug action, drug dose regimens, and treatment strategies.[4] Such studies will eventually provide the means to accomplish "personalized medicine" by monitoring individual responses to drug delivery. For diagnostic imaging, the half-life of the radionuclide must be long enough to carry out the chemistry of the desired radiopharmaceutical and allow its accumulation in the target tissue in the patient while the drug clears from the nontarget organs. Radiometals for pharmaceuticals used in PET and γ scintigraphy range in half-life from about 10 min (^{62}Cu) to several days (^{67}Ga). For example, heart or brain perfusion-based radiopharmaceuticals require shorter half-lives, since they reach the target quickly whereas tumor-targeted compounds often take longer to reach the target and to be accumulated for gaining optimal target-to-background ratios.[5]

In PET imaging,[18]F-FDG (^{18}F-fluoro-2-deoxyglucose) is widely used in the clinic for the assessment of glucose metabolism in the heart, lungs, and brain.[6−8] However,[18]FDG-imaging suffers from several limitations, such as the reduced specificity for tumor cells due to FDG uptake in inflammatory lesions, short half-life, etc. The longer half-life (4 days) of the ^{124}I-product(s) compared to 90 min for ^{18}F-FDG has a number of additional advantages: (i) patients do not have to go through another injection after surgery to view its effectiveness, (ii) imaging centers do not need to order a large number of vials, (iii) as a result of its long half-life, it can be transported over long distances and, therefore, could reduce the number of highly expensive cyclotrons, and, finally, (iv) not only does this mean an increased benefit to the end user (the patient), it also provides a significant benefit to insurance companies.

The design of a radiopharmaceutical agent requires optimizing the balance between specific in vivo targeting (e.g., cancerous tumor),

Received: June 21, 2011
Published: August 15, 2011

Scheme 1. Modification of Methyl Ester Functionality

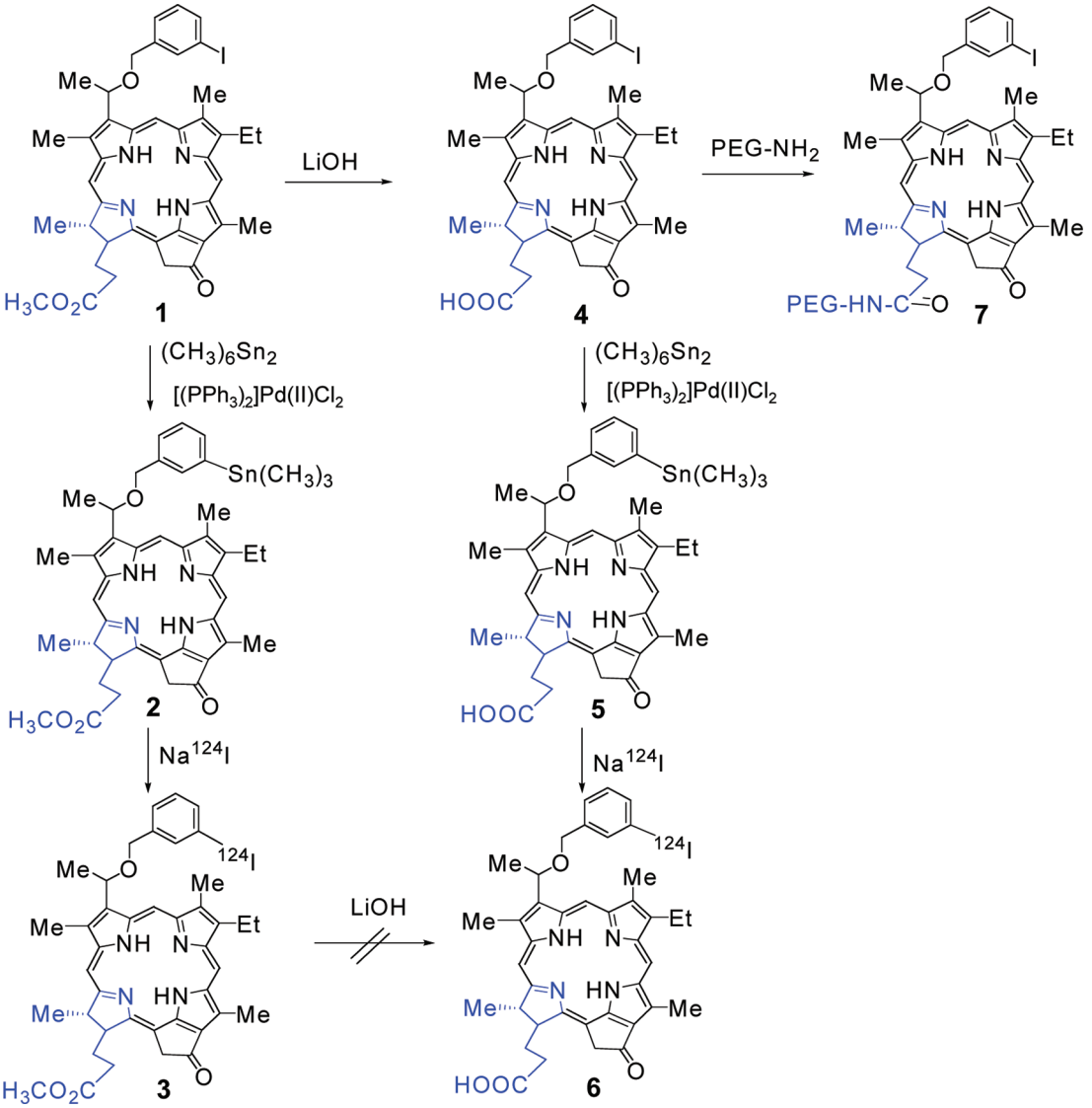

clearance from nontarget tissues/organs, as well as time-dependent application in line with the decay properties of the radionuclide.[9] Several considerations need to be made when designing selective radiolabeled drugs. These include efficient drug delivery, optimization of relative accumulation of the drug at the target over nontarget sites, maximizing the residence time of the radioactivity at target sites, and prevention of structural alteration of the drug.[10] Because of the multiple parameters that must be considered, developing effective radiopharmaceuticals for combined imaging and therapy of cancer is a challenging undertaking that is not simply solved by attaching a radionuclide in any fashion to a nonradiolabled targeting compound. At the very least, the radionuclide should not interfere with pharmacokinetics, binding specificity, or retention by cancer cells. The selection of the radionuclides and the chemical strategies for radiolabeling of molecules are critical elements for developing safe and improved imaging/therapeutic agents.[11]

For the last several years, one of the objectives of our laboratory has been to use porphyrin-based compounds for the treatment of cancer by PDT.[12,13] The accumulation of certain porphyrins and related tetrapyrrolic systems is higher in malignant tumors than in most normal tissues, and that has been the main reason to use these molecules as photosensitizer (PS). Some tetrapyrrole-based compounds have been effective in treating lesions at different organ sites, including skin, lung, bladder, head, and neck and esophagus.[14] The precise mechanism(s) of PDT and post-PDT reactions are still largely unknown; however, data from in vitro and in vivo studies suggested that localized oxidative damage mediated by PS-specified photoreactions determines direct cell killing, loss of vascular function, and post-PDT immune reactions, all of which play significant roles in PDT outcome.[15−20] Superficial lesions, or those that are endoscopically accessible, e.g. endobronchial or esophageal tumors, are easily treated. However, the majority of malignant lesions are too deep to be reached by light of the wavelength required to trigger singlet oxygen production by the current generation of PSs. Although the technology to deliver therapeutic light to deep lesions via optical fibers "capped" by a terminal diffuser is well developed, a deep lesion is by definition not visible from the skin surface and the precise PDT of deep tumors, thus far, has been

dx.doi.org/10.1021/jm200805y |J. Med. Chem. 2011, 54, 6859–6873

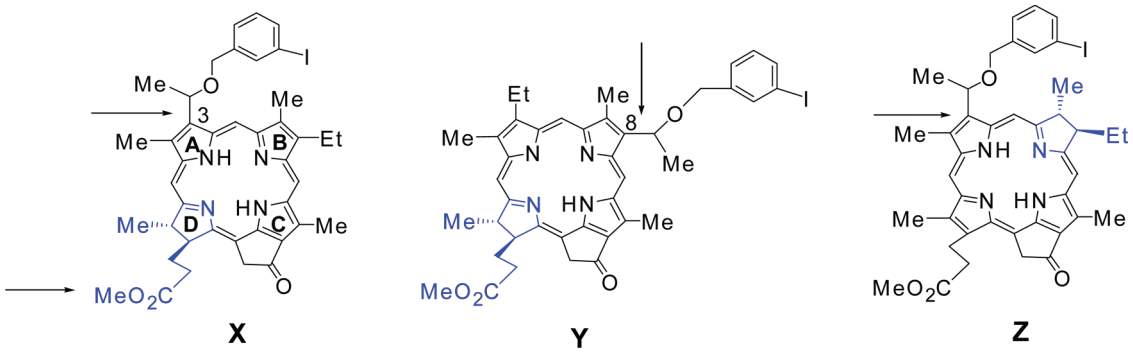

Figure 1. Various approaches of structural modification of iodinated PS: (**X**) modification of methyl ester functionality; (**Y**) effect of the position of the (1′-*m*-iodobenzyloxyethyl) substituent; (**Z**) effect of ring-B vs ring-D reduced PSs in biological efficacy.

impractical. However, nuclear imaging guided implantation of optical fibers within deep tumors would greatly enhance PDT.

On the basis of a SAR study of a series of alkyl ether analogues of pyropheophorbide-*a*, a relatively long wavelength absorbing PS, the 3-(1-hexyloxyethyl) derivative (HPPH).[21,22] has been developed in our laboratory, proved to be tumor-avid, and is currently in phase I/II multicenter human clinical trials.[23,24] Initially, we investigated the utility of HPPH as a "vehicle" for delivering the mono- or dibisaminoethanethiols (N_2S_2 ligand)[25] combined with technetium-99 m to tumors. The in vivo biodistribution data indicated that the tumor/nontumor uptake ratio of the conjugates correlated with time and tumor size. Its clearance from tumor was slower than that of most of the nontumor tissues. However, the short 6-h half-life of ^{99m}Tc was incompatible with a 24-h PS uptake time, suggesting that longer-lived isotopes, such as ^{111}In or ^{124}I, could provide a useful scanning agent. Among a series of radiolabeled PSs[25−28] investigated so far, the ^{124}I- labeled methyl 3-(*m*-iodobenzyloxyethyl)pyropheophorbide-*a* was found to be an effective PET/PDT imaging agent.

In our attempt to develop improved PDT agents, we have shown that (i) overall lipophilicity and (ii) the presence and position of various substituents in a variety of tetrapyrrolic systems related to pyropheophorbides, purpurinimides, and bacteriopurpurinimides have a significant impact on cellular uptake, intracellular localization, photoreaction, and PDT efficacy. Though the ^{124}I-labeled PS **3** (Scheme 1) containing a 3-(1′-*m*-iodobenzyloxyethyl) group at position-3 of the molecule showed promising tumor imaging (PET) ability, we were interested to determine whether an alternative position of the iodobenzyl group on the macrocycle or reduction of the B-ring in place of the D-ring would change the cell biology of the PS, such as cellular uptake and retention, that could then be exploited for designing tumor-specific PS delivery. To do so, we synthesized a series of related analogues by (i) modifying the methyl ester group of the propionic ester side chain, (ii) introducing the (*m*-iodobenzyloxyethyl) group at position-8 (instead of position-3), and (iii) preparing the corresponding ring-B reduced isomer (instead of ring-D) and investigating the biological consequences of these both in vitro and in vivo (Figure 1). We discovered that the position of the iodobenzyl group affects efficacy in uptake and retention of the PSs, whereas the carboxylic group at position-17^2 determines not only the quantitative amount of PS internalization but also the site of long-term intracellular retention. Interestingly, the mechanism of internalization and subcellular deposition of the PS radically changed by conjugating polyethyleneglycol (mol wt 5000) at position-17^2.

RESULTS AND DISCUSSIONS

Chemistry. The iodinated PS **1** containing the methyl ester functionality and the corresponding ^{124}I-analogue **3** were prepared by following the methodology developed in our laboratory[26] (Scheme 1). To investigate the effect of the polyethyleneglycol (PEG) moiety in cellular uptake and PDT efficacy, the PEG analogue **7** was synthesized in excellent yield. The corresponding isomer **11** containing a (1′-*m*-iodobenzyloxyethyl) group at position-8 and the corresponding carboxylic acid derivative **12** were prepared from the methyl pyropheophorbide-*a* **8** by following the methodology depicted in Scheme 2. During the preparation of the desired compound, methyl-8-vinylpyropheophorbide-*a* **16**, a byproduct in minor quantity, was also isolated, and the possible mechanism for the formation of the byproduct **16** is shown in Scheme 2. To investigate the impact of ring-B vs ring-D reduced isomers in tumor imaging and PDT efficacy, the desired labeled analogues containing either a propionic ester or a carboxylic acid side chain were synthesized from methyl bacteriopyropheophorbide-*a* **17**, which in turn was obtained from *Rb. sphaeroides*.[29] The reaction sequences followed for the preparation of the desired compounds are shown in Scheme 3. In brief, two approaches were used for the preparation of intermediate **20**. In the first approach, the bacteriochlorin **17** was reacted with sodium borohydride, and the resulting hydroxy ethyl derivative **18** was reacted with HBr gas, the intermediate bromo- analogue was not isolated and, after drying under vacuum (inert atmosphere), was immediately reacted with 3-iodobenzyl alcohol, resulting in bacteriochlorin **19**. For the preparation of ring-B reduced chlorin **20**, bacteriochlorin **19** was subjected to ferric chloride oxidation and the desired analogue was isolated in 70−75% yield. In the second approach, chlorin **21** in a sequence of reaction gave the corresponding 3-(*m*-iodobenzyloxyethyl) analogue **20** (Scheme 3). Starting from **20**, the ^{124}I-labeled analogues either as methyl ester **26** or carboxylic acid **27** were synthesized by following the methodology discussed for other isomers (Schemes 1). The structures of all the intermediate and the final products were confirmed by NMR, mass spectrometry, and elemental analyses. The purity was ascertained by HPLC. Radiolabeling efficiency and specificity of the labeled analogues both as methyl ester and carboxylic acid derivatives was 30−32%, and the specific activity was greater than 1 Ci/μmol.

Before evaluating these compounds for biological efficacy, the structures of ring-B vs ring-D reduced isomers were confirmed by ^{1}H NMR. The striking features observed between the ring-D and ring-B reduced chlorins are shown in Figure 2. In brief, the 13^2-H proton observed as an ABX pattern at δ 5.37 ppm in ring-D

dx.doi.org/10.1021/jm200805y |*J. Med. Chem.* 2011, 54, 6859–6873

Scheme 2. Synthesis of 8-(1′-*m*-Iodobenzyloxyethyl)pyropheophorbides 11 and 12 and the 8-Vinyl Analogue 16

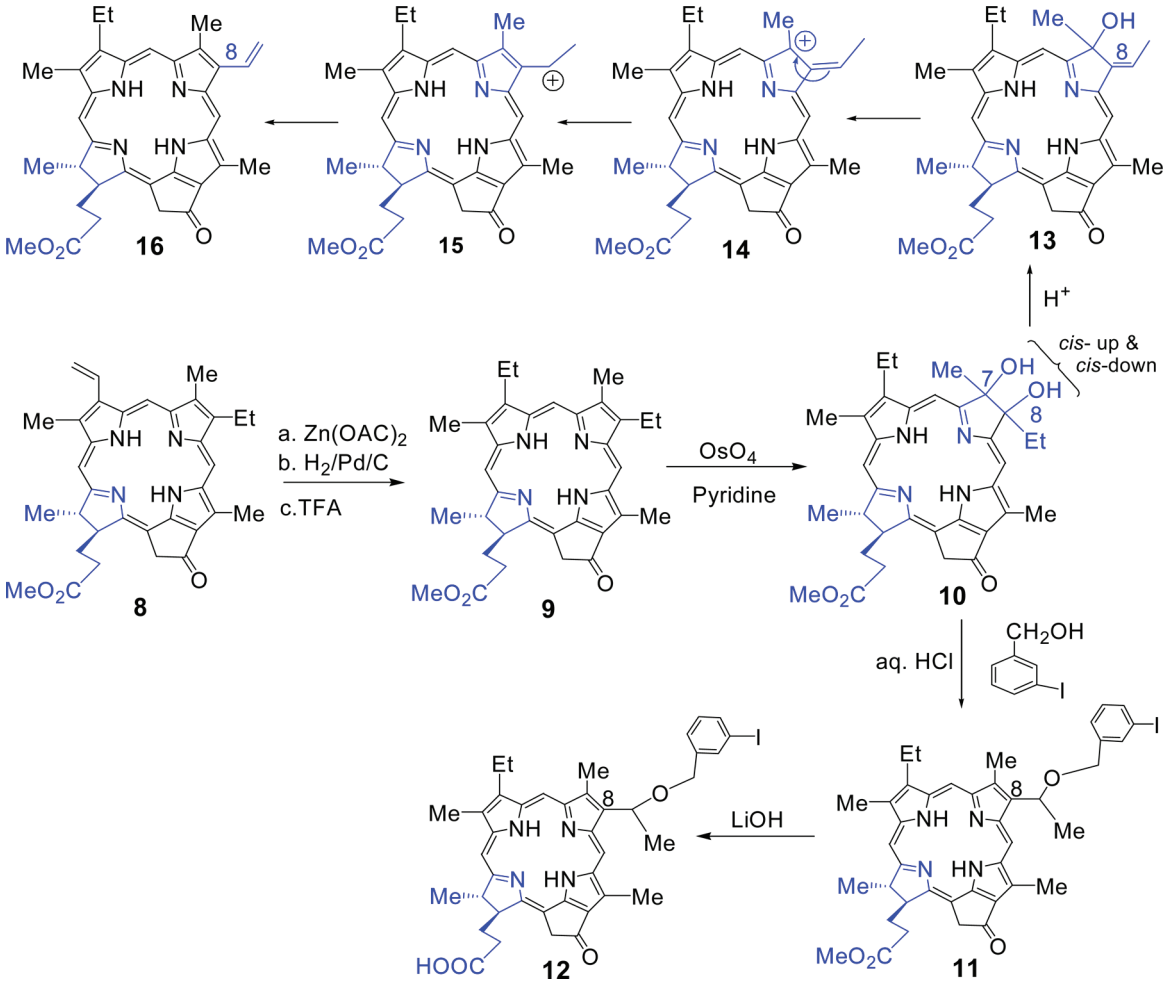

reduced chlorin **1** appeared as a singlet at 5.82 ppm in ring-B reduced chlorin **20**, suggesting a regioselective oxidation of ring-D, which was further confirmed by the presence of triplets at δ 4.25 and 3.33 ppm, each integrating for two protons and assigned to the 17^1- and 17^2-CH_2 protons of the propionic ester side chain, whereas, in ring-D reduced chlorin, these protons were observed at δ 2.51, 2.35, and 2.05 ppm, respectively. The *meso*-region of both the chlorins showed interesting features. For example, the 5-H proton appearing at δ 9.62 for chlorin **1** was observed at 9.21 ppm for the ring-B reduced isomer **20**. The 20-*meso* proton, which appeared at δ 8.46 ppm in D-ring reduced chlorin **1**, was observed at δ 8.65 in isomer **20**. Compared to the case of the ring-D reduced isomer, the resonances of **20** at δ 9.01 ppm integrated for a single proton assigned to the 10-*meso* proton appeared at δ 9.21 ppm in chlorin **1**, possibly as a result of higher electron density at these positions (see the Supporting Information).

The course of reaction for the preparation of the intermediates and final products for the synthesis of the isomeric structures **1**, **11**, and **20** (or the corresponding carboxylic acids **4**, **12**, and **23**, respectively) could be followed by monitoring changes in the absorption spectrum. The following interesting differences between the electronic spectra of the ring-B and ring-D reduced isomers were observed: As shown in Figure 3, the isomers **4** and **12** containing an iodobenzyloxyethyl group at position-3 or position-8 of the chlorin system showed almost identical electronic absorption spectra (long wavelength absorption 660 nm (CH_2Cl_2)); however, the ring-B reduced chlorin **23** exhibited the long wavelength absorption at λ_{max} 670 nm. No significant difference in singlet oxygen yields was detected between the ring-B and ring-D reduced isomers, and they ranged from 0.45 to 0.48.

The rate of photobleaching of isomers **4**, **12**, and **23** was also investigated in 17% bovine calf serum (BCS) in equimolar concentration. As can be seen from Figure 3B, all isomers showed almost 50% photobleaching on exposing the photosensitizers to light (75 mW/cm^2) for 20−22 min. Interestingly, on further irradiation, the rate of photobleaching of **12** (ring-D reduced chlorin containing the 1′-benzyloxyethyl group at position-8) was slightly slower than those of the other two isomers, suggesting its increased photostability.

Biological Studies. The initial functional assessment of the PSs (cellular uptake, intracellular localization, STAT3 dimerization, and PDT efficacy) was carried out in the cell culture model of human basal cell carcinoma (BCC1). The relative PDT efficacies determined in these cells were then evaluated in the mouse colon adenocarcinoma cell line (Colon26) grown in vitro and as subcutaneous tumors in BALB/c mice.

Correlation between Cellular Uptake, STAT3 Dimerization, and Cell Killing. The cell biological properties of the iodinated PS

dx.doi.org/10.1021/jm200805y |*J. Med. Chem.* 2011, 54, 6859–6873

Scheme 3. Synthetic Approaches for the Preparation of Ring-B Reduced 3-(1′-*m*-Iodobenzyloxyethyl) Chlorins from Bacteriopyropheophorbide-*a*

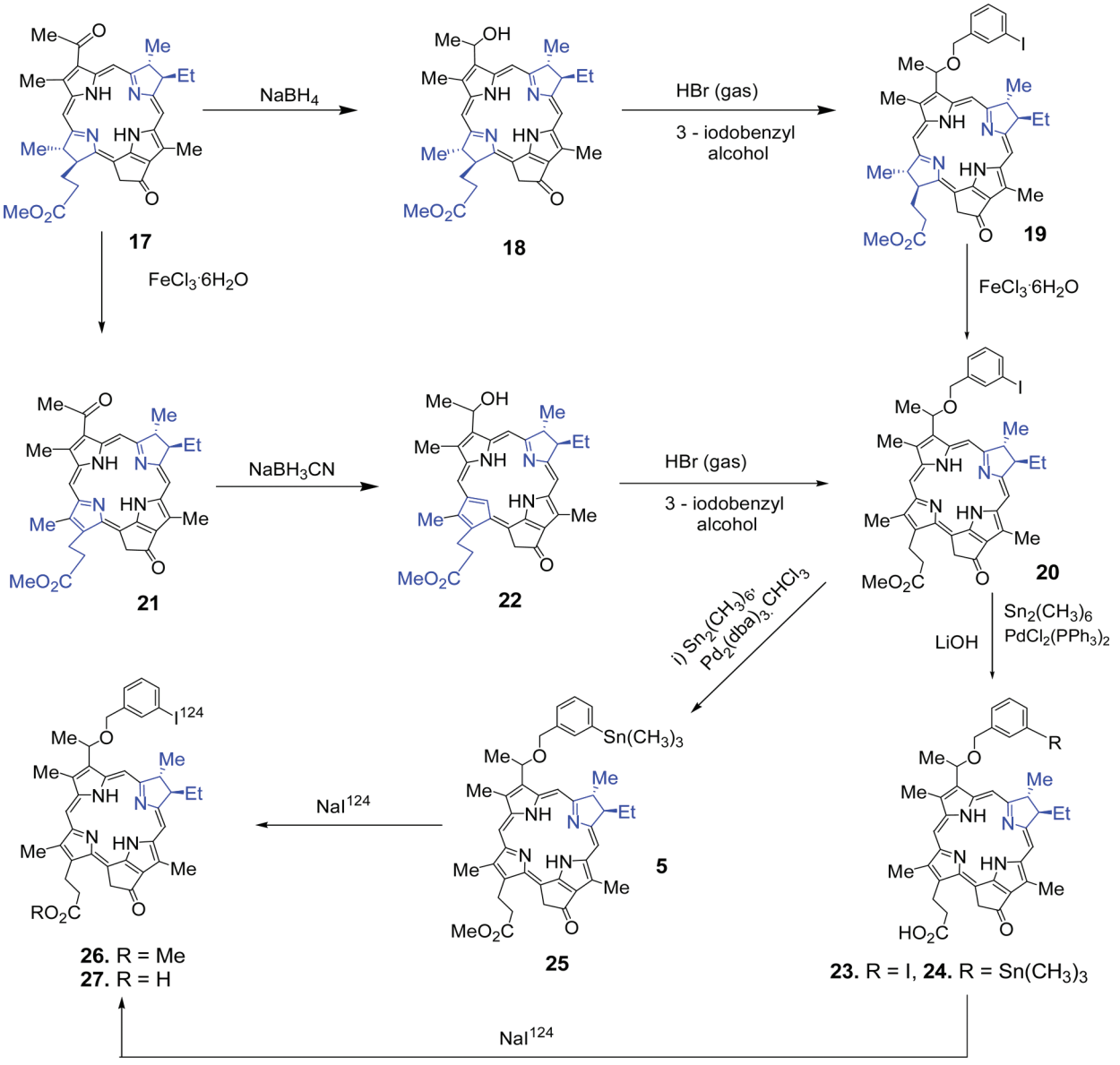

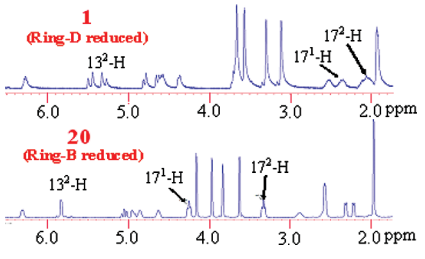

Figure 2. ^{1}H NMR spectra of ring-D vs ring-B reduced chlorins **1** and **20**, respectively.

1 were evaluated as a function of derivatization at position 17^2 to carboxylic acid (PS **4**) or conjugated with PEG (polyethylene glycol, mol wt 5000) (PS **7**). The same cellular characterization determined the impact of the iodobenzyl group added to position 8 (PS **12**) or B-ring reduction (PS **23**) in the carboxylic acid PS derivatives. Incubation of BCC1 cells with these PSs for 30 min allowed assessment of immediate uptake (Figure 4A). The cellular distribution of the PS fluorescence indicated that PS **4** was efficiently taken up and deposited into the mitochondrial compartment. Both the B-Ring reduction (PS **23**) and placement of the iodobenzyl group to position-8 (PS **12**) in the carboxylic acid derivatives lowered the cellular uptake by 2-fold and 4-fold, respectively, relative to the case of PS **4**. The subcellular localization was identical for all three PSs and was not altered as a function of continued incubation of the cells in PS-free medium for 4−24 h (data not shown). However, as found for other porphyrin-based PSs, cell-associated PS **4**, **12**, and **23** were lost with a ∼4−5-fold higher rate when the cells were cultured in medium containing 10% serum compared to cells cultured in serum-free medium (data not shown). Strikingly different was the >100-fold lower uptake of

dx.doi.org/10.1021/jm200805y |*J. Med. Chem.* 2011, 54, 6859–6873

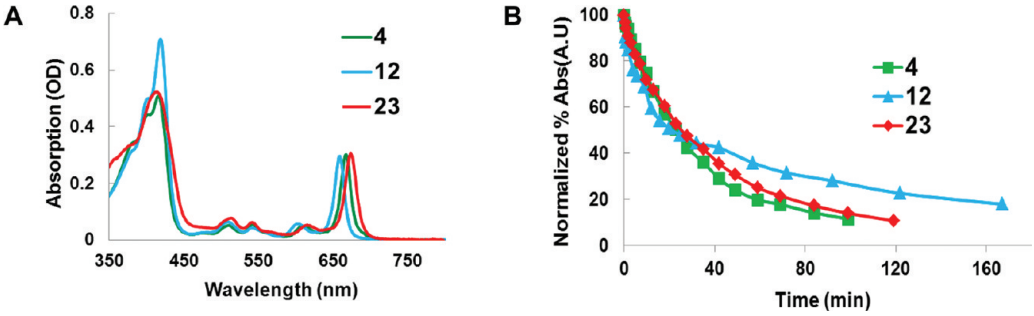

Figure 3. (A) Electronic absorption spectra of isomers **4**, **12**, and **23** at equimolar concentration (6.5 μM) in 17% bovine calf serum (BCS). (B) Rate of photobleaching of bacteriochlorins **4**, **12**, and **23** in 17% BCS. The photosensitizers at equimolar concentration (6.5 μM) were irradiated with light (light dose: 75 mW/cm^2), and the spectra were taken at variable time points. The normalized long wavelength absorption values were plotted with time, showing a comparative rate of photobleaching of the photosensitizers by reactive oxygen species (mainly singlet oxygen) produced in situ.

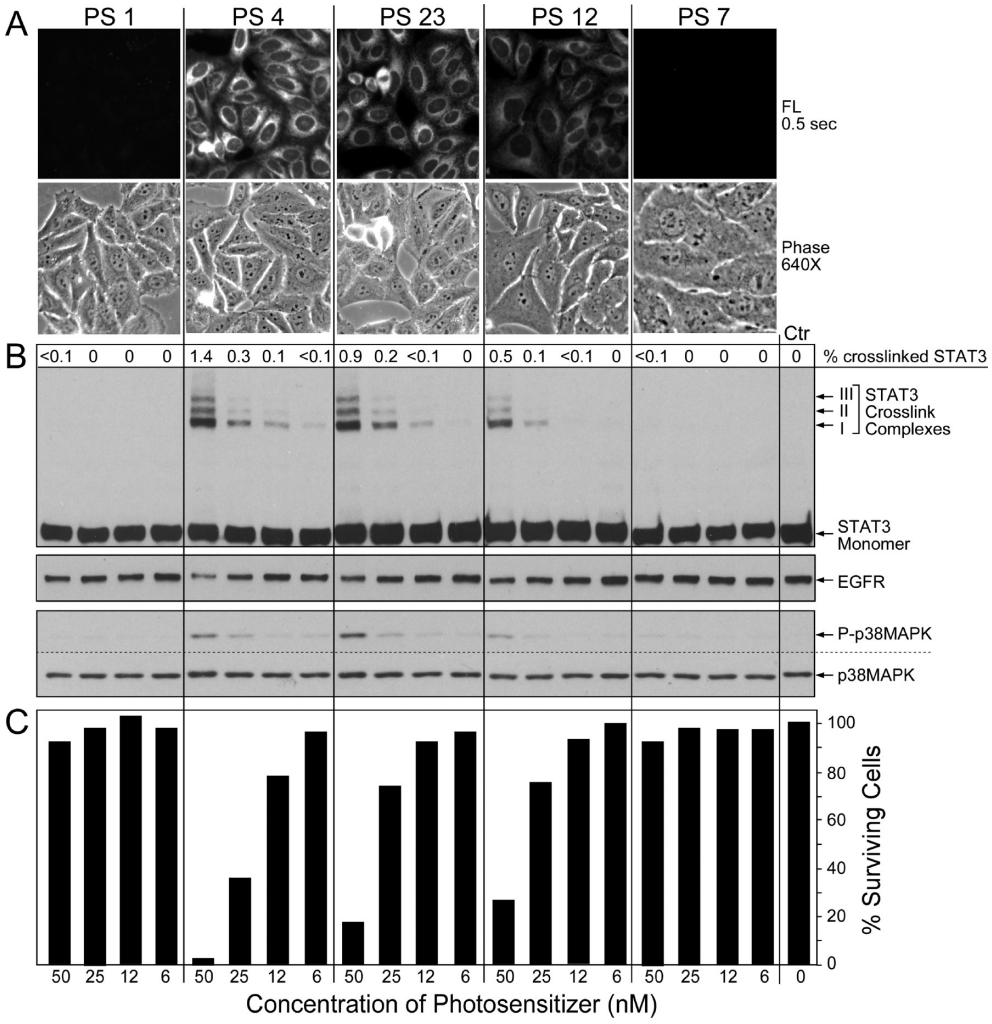

Figure 4. PS-specific uptake, photoreaction, and post-PDT survival. Replicate 24-well culture plates of BCC1 cells were incubated for 30 min in serum-free DMEM containing 200 nM (A) or for 2 h with serum-free DMEM containing 2-fold serially diluted preparations (B and C) of the PSs indicated at the top. The cells were washed free of PS and imaged at 640× magnification under phase contrast and HPPH fluorescence (A). The plates treated with the serially diluted PSs were illuminated for 9 min with 665 nm light, yielding a fluence of 3 J/cm^2. The cell monolayers in one culture plate were immediately extracted. Equal aliquots of the extracts were analyzed on Western blots for the levels of immune detectable STAT3, EGFR, and phosphorylated and total p38 MAPK (B). The oxidative cross-linking of STAT3 was determined by densitometric scanning of the bands representing monomeric and homodimeric complex I. The percent conversion of STAT3 to the dimeric form is indicated at the top of panel "B". The second culture plate was changed to DMEM containing 10% fetal calf serum immediately after light treatment and cultured for an additional 24 h period. The number of surviving, trypan blue-excluding cells were counted in a hemocytometer and expressed relative to the number of cells in the control (C).

dx.doi.org/10.1021/jm200805y |J. Med. Chem. 2011, 54, 6859–6873

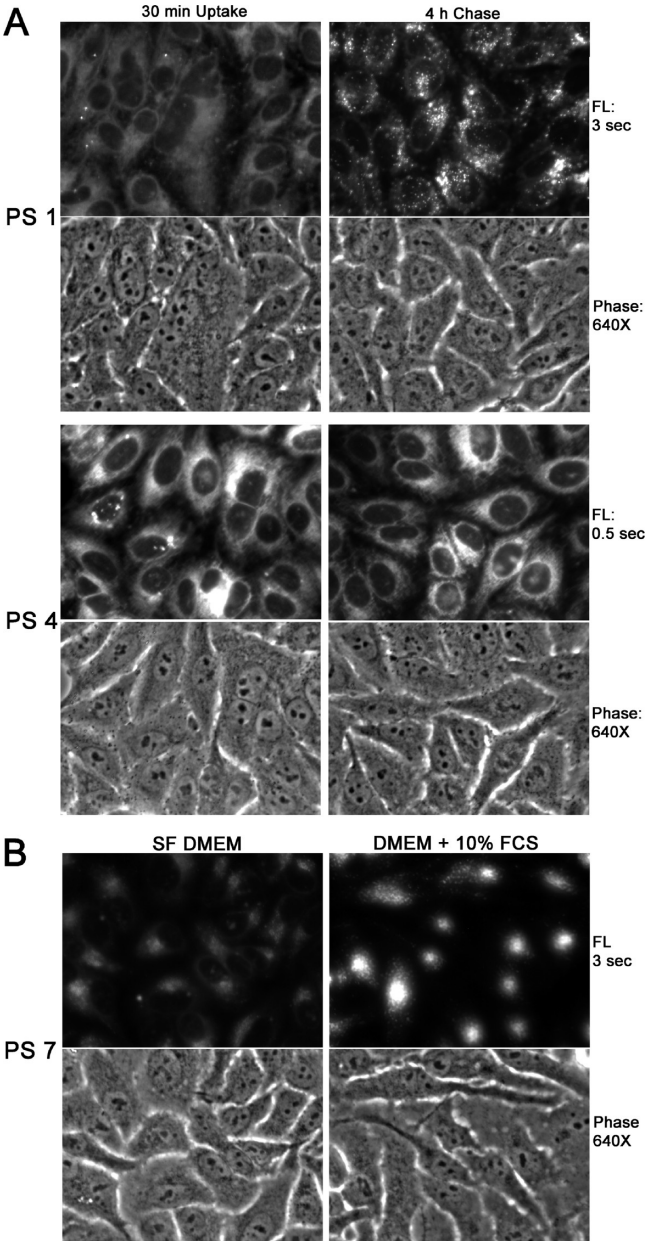

Figure 5. Specific patterns of uptake and subcellular distribution of the PSs. (A) BCC1 cells were incubated for 30 min in serum-free DMEM containing 3.2 μM PS **1** or 0.2 μM PS **4**. The cells were washed, and images of the cell monolayers were recorded at 640× magnification under phase contrast or HPPH fluorescence. The cultures were incubated in PS- and serum-free DMEM for an additional 4 h period. The cells were imaged again under identical condition as before. (B) BCC1 cells were incubated for 24 h in either serum-free DMEM or DMEM with 10% fetal calf serum, both containing 3.2 μM PS 7. The cells were washed free of PS and imaged at 640× magnification.

the methyl ester derivative, PS **1**, and the PEGylated PS **7** relative to PS **4** (Figure 4A). The quantitative difference in uptake and retention was also evident following incubation of the cells with the PSs for 2 h, although the overall level of cell-associated PSs was enhanced (data not shown).

Treatment of the PS-incubated cells with therapeutic light mediated photoreactions that were strictly proportional to the level of PS as determined by fluorescence. The photoreactions were manifested in the level of STAT3 cross-linking, loss of EGFR protein, and activation of the stress MAPK, p38 (Figure 4B). The same PDT treatment also led to a PS dose-dependent cell killing as determined by the fraction of the cells surviving 24 h post-PDT-incubation (Figure 4C). Under the conditions used in Figure 4, the cellular uptake of PS **1** and PS **7** was barely detectable by fluorescent microscopy, and the low levels of PS were ineffective in mediating photoreactions that were quantifiable by the biochemical markers. By increasing the concentrations of the PSs in cell treatments, we detected that the two PSs displayed fundamentally different modes of uptake and subcellular localization compared to the carboxylic acid-containing PSs. A time course analysis indicated that, within the 30 min incubation period, a low-level of PS **1** was accumulated in the mitochondrial compartment, yielding a pattern as observed for PS **4** (Figure 5A, left panel). However, during a subsequent 4 h incubation period in PS-free medium, a major fraction of the cell-associated PS fluorescence was redistributed and retained at new subcellular sites that include the lysosomal compartment, whereas PS **4** maintained the initial mitochondrial localization (Figure 5A, right panel). The uptake of PS **1**, as PS **4**, was subject to competition with serum protein, with ~5-fold lower fluorescence recorded for cells incubated with PS **1** in the presence of 10% fetal calf serum (data not shown). The opposite uptake properties in the presence of serum proteins were detected for PS **7**. The PEGylated PS **7** was synthesized to identify whether this hydrophilic version of the PS will reduce hepatic clearance and, thus, enhance the availability for uptake by tumor in vivo. Short-term incubation of basal cell carcinoma (BCC1) cells with PS **7** indicated that PS **7** uptake was very low, with levels below microscopic detection (Figure 4A). Only at higher input concentrations and prolonged incubation, i.e., 24 h, could an increased and time-dependent cellular accumulation be observed (Figure 5B, right panel). Unexpectedly, the cellular uptake was several-fold higher in the presence of serum proteins (Figure 5B, right panel). The subcellular localization, regardless of the incubation conditions, was exclusively the endosomal/lysosomal compartment. Since PS **7**, unlike other lysosomally targeted PSs, such as HPPH-Gal,[30] did not show any binding to cell surface internalization, we concluded that the uptake of PS **7** was not through the route of first binding to the plasma membrane followed by endocytosis but largely through fluid phase pinocytosis.

Differential Functions of the PSs Are Reproducible in Murine Colon26 Tumor Model. The relative activities of the PSs determined in BCC1 cells were confirmed in the mouse tumor cell lines Colon26. The comparative study involved two separate sets of experiments. In the first set, Colon26 cells were incubated for 24 h in serum-containing culture medium with either PS **1**, **4**, or **7**. The duration of PS treatment was extended to 24 h in order to enhance intracellular accumulation of the PSs, in particular PS **1** and **7**. Following the photoreaction at increasing light doses and culture in growth medium for an additional 24 h, the surviving Colon26 cells were evaluated by MTT assay (Figure 6A). The relative PDT efficacy of the PSs followed the patterns determined in BCC1 cells (Figure 4C), with PS **4** as the most effective PS. The second experimental set determined the efficacy of PS **4** with the other isomers, PS **12** and PS **23** (Figure 6B). All three isomers showed comparable in vitro efficacy that in part was due to the application of higher PS concentration. Measurement of PS uptake by Colon26 cells showed comparable values (PS **4** ≥ **23** > **12**) as found in

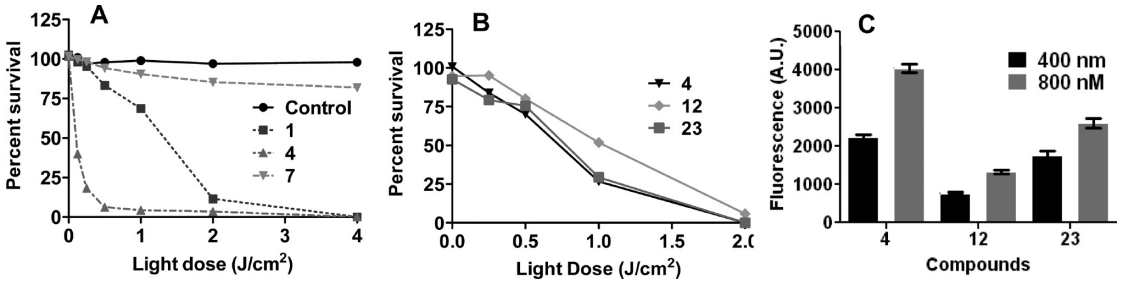

Figure 6. (A) In vitro photosensitizing efficacy of PS **1**, **4**, and **7**. (B) PS **4**, **12**, and **23**. Colon26 cells were incubated with 0.3 μM (A) and 0.0625 μM (B) of PSs, respectively, in growth medium for 24 h. The cells were treated at the peak absorption wavelength with variable light doses and cultured for an additional 48 h post-treatment. (C) PS uptake of compounds **4**, **12**, and **23** in Colon26 cells 24 h postincubation was determined by flow cytometry.

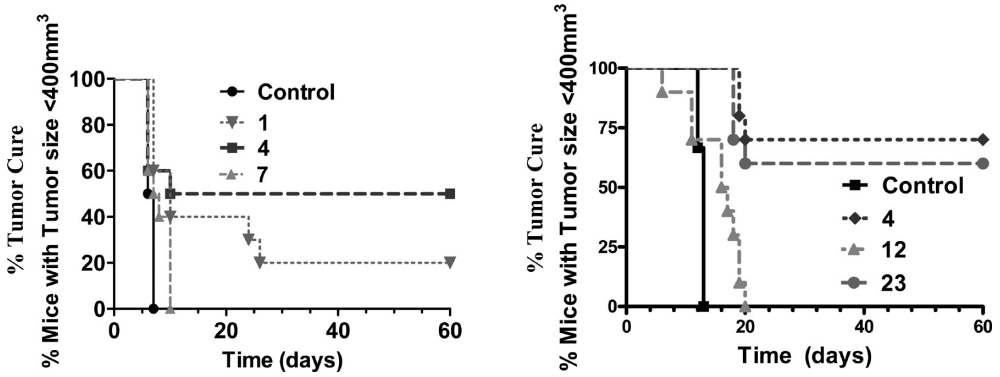

Figure 7. (A) Comparative in vivo photosensitizing efficacy of PS **1**, PS **4**, and PS **7** and (B) PS **4**, **12**, and **23** in BALB/c mice bearing Colon26 tumors (10 mice/group). The mice were injected with photosensitizers (1.00 μmol/kg), and the tumors were exposed to laser light at 665 nm for compounds **1**, **4**, and **7**; 674 nm for compound **23** and 660 nm for compound **12** (light dose: 128 J/cm^2, 14 mW/cm^2) at 24 h postinjection. At day 60, photosensitizers **4** and **23** gave 70% and 60% tumor response, respectively (7/10 and 6/10 mice were tumor free), whereas compound **12** showed limited efficacy.

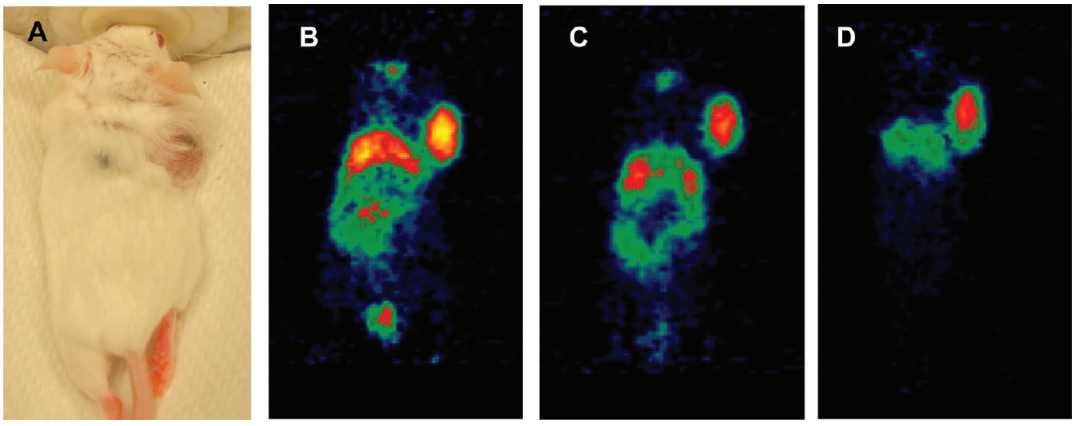

Figure 8. Whole-body PET images of a BALB/c mouse bearing Colon26 tumor with ^{124}I-PS **6** (A) taken at 24, 48, and 72 h postinjection. The maximum uptake of the PS was observed at 24 h postinjection. However, the best contrast was obtained at 72 h for compound PS **6** postinjection.

BCC1 cells (Figures 4C and 6C). On the basis of the in vitro findings, the relative activity of the PSs in mediating Colon26 tumor treatment in vivo was determined. PS **1**, **4**, and **7** were administered at a dose of 1.0 μmol/kg to BALB/c mice bearing subcutaneous Colon26 tumors. After 24 h, the tumors were exposed to light (128 J/cm^2, 14 mW/cm^2). The animals were monitored for 60 days for recurring tumor growth (Figure 7A). In line with the relative activities determined in cell culture, PS **4** gave 50% tumor cure whereas PS **1** was significantly less effective and only 20% cure mice were tumor-free on day 60. Under these treatment parameters, PS **7** was ineffective. We interpret the substantial in vivo activity of PS **1** to be the result of progressive PS **1** accumulation in the tumor during the 24 h period postinjection and to possibly involve the mode of cellular uptake detected in cultured cells (Figure 5A). A second series of in vivo tumor treatments tested the activity of PS **23** and PS **12** relative to PS **4** (Figure 7B). PS **4** and PS **23** showed relative efficacy that matches those detected for these two PSs in vitro (Figures 4C and 6B).

Comparative PET Imaging Ability of Photosensitizers 3 and 6. As evident from the tissue culture experiments and in vivo

dx.doi.org/10.1021/jm200805y |J. Med. Chem. 2011, 54, 6859–6873

tumor treatments, PS **4** displayed the highest PDT efficacy, followed by PS **23** and **12**. We have previously shown that the ^{124}I-labeled methyl ester derivative of PS **1**, PS **3**, showed a great potential for imaging tumors in BALB/c mice bearing Colon26 tumors. In light of the new finding regarding the activity of PS **4** and our goal to develop a "multifunctional agent" based on optimized PS structures for efficient tumor-imaging and therapy, we compared the tumor-imaging and biodistribution of PS **3** with the corresponding ^{124}I-labeled form of PS **4**, PS **6**. Similar to the methyl ester derivative,[26] PS **6** showed significant tumor uptake at 24, 48, and 72 h postinjection (Figure 8). Compound PS **27** showed a similar uptake profile as compared to that of PS **6** (data not shown). The corresponding methyl ester derivative of compound PS **27** and its ^{124}I-labeld form, PS **26**, also exhibited a similar uptake profile as compared to that of compound PS **3** (data not shown). With both analogues, the maximal tumor uptake was observed at 24 h postinjection, as determined by region of interest (ROI) calculations. However, for imaging, 72 h postinjection for compounds PS **4** and **6** and compound PS **27** (data not shown) produced the best contrast, as the compounds cleared more rapidly from liver, spleen, and intestine than from the tumor (Figure 8). The accumulation of label in the thyroid due to release of free ^{124}I could be blocked by injecting cold potassium iodide in water 24 h prior to injecting the labeled photosensitizer (data not shown).

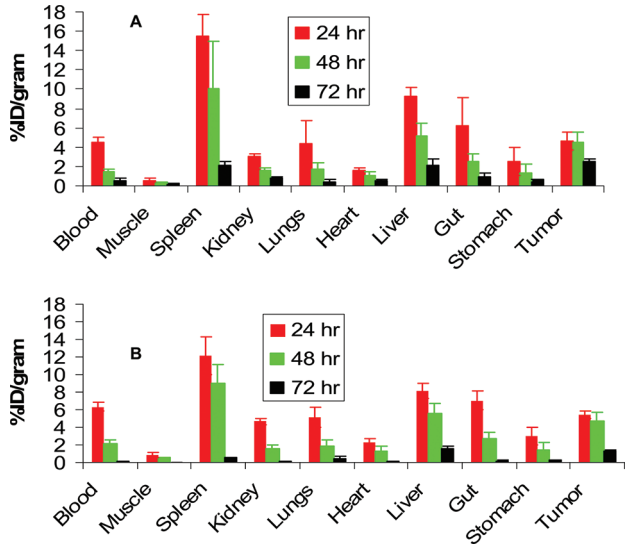

Figure 9. Comparative biodistribution of ^{124}I following injection of PS **3** (A) and PS **6** (B) (100 μCi) in BALB/c mice bearing Colon26 tumors (three mice/time point) at 24, 48, and 72 h postinjection. Replacing the methyl ester functionality in PS **3** with a carboxylic acid functionality (PS **6**) did not make much difference in uptake of the PS in tumor and other organs, except the spleen, where the uptake was significantly reduced.

Comparative in Vivo Biodistribution of PS 3, PS 6, and ^{18}F-FDG. Among the isomers investigated for PDT efficacy, PS **4**, the pyropheophorbide-*a* containing *m*-iodobenzyloxyethyl at position-3 of the ring-D reduced chlorin system and with a carboxylic acid group at the 17^2-position, was found to be most effective. Interestingly, PS **1**, the derivative bearing an ester functionality, despite its lower PDT efficacy, showed remarkable tumor imaging ability.[26] For determining the relative tumor uptake and other organ uptake, we compare the in vivo biodistribution of ^{124}I following injection of both PS **3** and **6** into BALB/c mice bearing Colon26 tumors. Specifically, a set of nine tumor-bearing mice were injected with each compound (50 μCi), and three mice per group were imaged after 24, 48, and 72 h for 30 min with microPET. Following imaging, the mice were sacrificed and specific radioactivity values in individual organs (% injected dose per gram) were determined (Figure 9). Both PSs showed similar biodistribution and clearance from all the organs, with the notable exception of slightly higher spleen-uptake of PS **1**. ^{124}I-labeled PS **27** (B-ring isomer) also demonstrated similar tumor uptake as compared to PS **6** (Figure 9A) but showed significantly lower spleen uptake (data not shown).

Among the PET imaging agents, ^{18}F-FDG is a current clinical standard, with the several limitation of short-term uptake processes. To assess the usefulness of PS **3** or PS **6** as alternative PET agents to FDG, we also determined the biodistribution of ^{18}F-FDG (isotope half-life 110 min) in BALB/c mice bearing Colon26 tumors. In brief, ^{18}F-FDG (150 μCi) was injected iv into three tumor-bearing mice, imaged by a PET scanning at 2 h postinjection. Mice were then sacrificed, and the specific radioactivity in the various organs was measured (Figure 10). The results indicated substantially different organ distribution than those for PS **3** and PS **6**, with higher uptake in muscle and heart relative to tumor.

Isomers 4, 12, and 23 Showed a Direct Correlation between Tumor-Uptake and Fluorescence Imaging. For investigating the fluorescence imaging potential of the isomers, the PS **4**, **12**, and **23** were injected intravenously (1.0 μmol/kg) in BALB/c mice (3 mice/group) bearing Colon26 tumors. For best visualization, the tumors were grown subcutaneously on the right shoulder to a size of 4−5 mm in diameter. The fluorescence in intact animals was imaged using the Nuance camera system at 24, 48, and 72 h postinjection. The images were then analyzed by generating false color images representing the fluorescence intensity of the drug at the tumor site. Among all the isomers investigated, the PS **4** (ring-D isomer) and **23** (ring-B isomer) showed similar drug uptake at 24, 48, and 72 h postinjection (p.i.) (Figure 11a and c). This could explain the similar in vivo photosensitizing efficacy of the two PS. Both PSs also showed

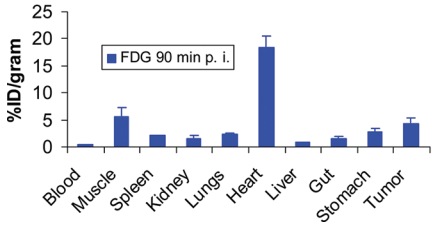

Organs	Uptake Ratio	Organs	Uptake Ratio
Tumor/Blood	11.4	Tumor/Stomach	1.49
Tumor/Muscle	0.77	Tumor/Gut	2.79
Tumor/Spleen	2.01	Tumor/Liver	5.15
Tumor/Kidney	2.87	Tumor/Heart	0.23
Tumor/Lungs	1.73		

Figure 10. Biodistribution of ^{18}F-FDG in BALB/c mice (3 mice/group) bearing Colon26 tumors at 2 h postinjection. The tumor uptake ratio is also presented in tabulated form.

dx.doi.org/10.1021/jm200805y |J. Med. Chem. 2011, 54, 6859–6873

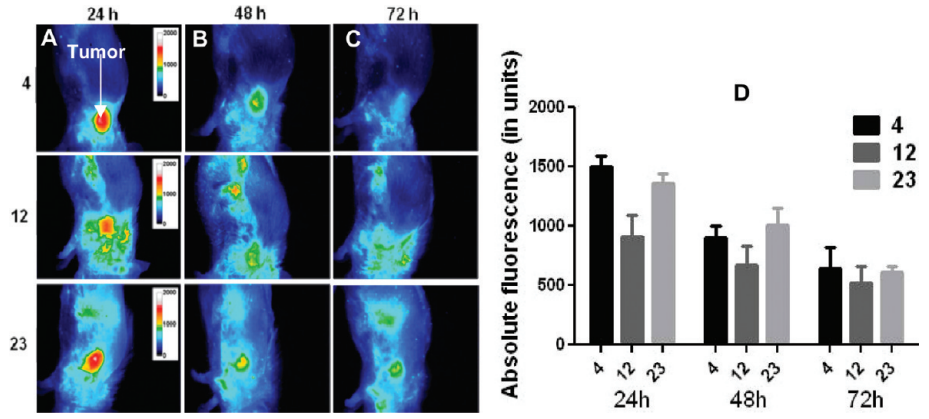

Figure 11. Whole body fluorescence reflectance images (FRI) of representative BALB/c mice implanted with C-26 tumors on the shoulder with compounds **4**, **12**, and **23**, respectively, at variable time points with a therapeutic dose (1 μmol kg^{-1}): (A) 24 h p.i.; (B) 48 h p.i.; (C) 72 h p.i. (D) average fluorescent intensity (AFU) of 3 mice ± SD of a ROI (20 mm diameter) over the tumor in AU, arbitrary units.

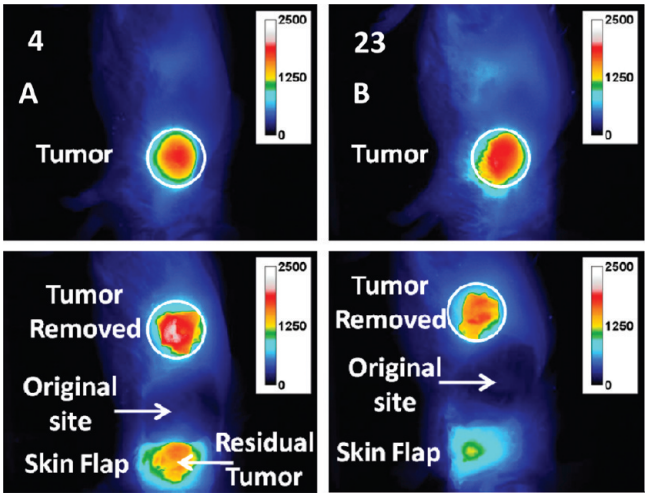

Figure 12. Whole body fluorescence reflectance images (FRI) of representative BALB/c mice implanted with Colon26 tumors on the shoulder with compounds **4** and **23** at 24 h postinjection (dose: 1 μmol kg^{-1}). λ_{ex} = 665 and 674 nm for PS **4** and **23**, respectively; λ_{em} = 710 nm). (A) PS **4**; (B) PS **23**; tumor was removed and skin was flapped back to expose the residual tumor. The two PSs **4** and **23**, exhibiting the highest in vivo phototoxicity, were injected intravenously into mice bearing Colon26 tumors to confirm that the recorded fluorescence coincided with the actual tumor mass. After 24 h, the tumors were surgically removed from the primary tumor site and imaged separate from the animal. The skin that covered the tumor was exposed to the camera, and the site along the tumor was imaged. The results clearly indicate that most of the fluorescence was confined to the tumor with only low fluorescence associated with the skin section.

similar clearance rates at 48 and 72 h p.i. (Figure 11d). PS **12** showed lower tumor uptake at 24 h compared to PSs **4** and **23** (Figure 11b), which is in agreement with the low accumulation in cultured cells (Figure 4) and tumor phototoxicity exhibited by PS **12** (Figure 7).

To study the potential of these agents as tumor imaging agents, the most effective compounds, PS **4** and **23**, were injected into mice bearing Colon26 tumors at the therapeutic dose of 1 μmol/kg. Twenty four hours post injection, the animals were sacrificed, and the primary tumor was removed surgically and imaged for fluorescence. The skin beneath the tumor was also exposed to light to see if any fluorescence was associated with skin mass. The results clearly showed the tumor avid nature of compounds of PS **4** and **23** (Figure 12). Most of the fluorescence was displayed from the tumor with little fluorescence associated with the skin. This might be useful to identify tumor mass from normal tissue mass during surgical removal of tumors.

CONCLUSIONS

In summary, the results obtained from a series of iodinated PSs suggest that a carboxylic acid group at position 17^2 favors a significant increase in cellular uptake by diffusion and deposition into the mitochondrial compartment, thereby increasing *in vitro/in vivo* PDT efficacy. In contrast, the same PS but with a methyl ester at position 17^2 displays low level cellular uptake and is subjected to a yet to define intracellular redistribution. Linking the PEG moiety (mol wt: 5000) to position-17^2 changes the PS to a hydrophilic molecule that assumes a behavior common to plasma constituents that are to be taken up by cells through fluid phase pinocytosis and deposited in the endosomal/lysosomal compartment. Interestingly, the isomer **12** in which the *m*-iodobenzyloxyethyl group was substituted at position-8 showed limited PDT efficacy. However, the isomer **23** in which the *m*-iodobenzyloxy was present at position-3, but instead of ring-D (PS **4**) the ring-B was reduced, was equally effective. The function/structure analysis of these photosensitizers demonstrated the close relationship of PS concentration in cells, PS-mediated photoreaction resulting in STAT3 dimerization, and PDT efficacy. These activities defined in vitro proved to a large extent to be predictive for the PS's action in vivo and also confirmed activities reported for other photosensitizers.[31] The ^{124}I-analogues of the effective PS also showed a great potential to function as tumor-imaging agent. PSs **1** and **4** were successfully applied to image tumors by PET and fluorescence. Detailed toxicological studies of these compounds in a good laboratory practice (GLP) facility following the United States Food and Drug Administration (US-FDA) guidelines are currently in progress.

EXPERIMENTAL SECTION

Chemistry. All chemicals were of reagent grade and used as such. Solvents were dried using standard methods. Reactions were carried out under nitrogen atmosphere and were monitored by thin-layer chromatography and/or UV−visible spectroscopy. Preparative scale thin-layer

chromatography was carried out on 20 × 20 cm^2 glass plates coated with Merck G 254 silica gel (2 mm thick). ^1H and ^{13}C NMR spectra were recorded on a Bruker AMX 400-MHz or Varian 400 NMR spectrometer at 303 K in $CDCl_3$ or ~10% CD_3OD in $CDCl_3$ or DMSO-d_6. Proton chemical shifts (δ) are reported in parts per million (ppm) relative to $CDCl_3$ (7.26 ppm) or TMS (0.00 ppm). Coupling constants (J) are reported in Hertz (Hz) and s, d, t, q, p, m, and br refer to singlet, doublet, triplet, quartet, pentet, multiplet, and broad, respectively. Mass spectral data (electrospray ionization, ESI by fusion) were obtained from Bioploymer facility, RPCI. The high resolution mass spectrometry analyses were performed at Mass Spectrometry Facility, Michigan State University, East Lansing, MI. CHN analyses were done at Midwest Microlab LLC, Indianapolis, IN. UV−visible spectra were recorded on a Varian Cary 50 Bio UV−visible spectrophotometer using CH_2Cl_2/MeOH as solvent. Melting points were uncorrected and were measured on a Thomas/Bristonline microscopic hot stage apparatus. In general most of the products obtained after column or preparative chromatography were crystallized/precipitated from dichloromethane/hexane. The purity of the compounds was confirmed by HPLC, and all compounds were >95%. The HPLC profiles of the final products are included in the Supporting Information.

Synthesis of 3-Devinyl-3-{1′-(*m*-iodobenzyoxy)ethyl}pyropheophoride-*a* (4). Methyl 3-devinyl-3-{1′-(*m*-iodobenzyoxy)ethyl}pyropheophoride-*a* (**1**) (150 mg, 0.19 mmol) obtained following the procedure developed by our group[26] was reacted with 240 mg (10.04 mmol) of aqueous LiOH in THF, and the reaction was stirred at room temperature overnight. The reaction mixture was neutralized with 2% AcOH in H_2O, and compound was extracted with CH_2Cl_2. The organic layer was washed with H_2O, dried over Na_2SO_4, concentrated, and precipitated with hexanes to yield the proposed compound (yield: 80%), mp: 138−140 °C. UV−visible, λ_{max} (MeOH/CH_2Cl_2), nm (ε): 663 nm (4.75×10^4), 605 (6.81×10^3), 539 (6.81×10^3), 506 (6.61×10^3), 411 (9.52×10^4). ^1H NMR ($CDCl_3$; 400 MHz): δ 9.62, 9.21, and 8.46 (three s, each for 1H, meso-H), 7.67 (s, 1H, ArH), 7.558 (d, J = 8.0, 1H, ArH), 7.183 (m, 1H, ArH), 6.962 (m, 1H, ArH), 5.867 (q, J = 6.8, 1H, 3^1-H), 5.16 (d, J = 18.6, 1H, 13^2-CH_2), 4.97 (d, J = 18.6, 1H, 13^2-CH_2), 4.62−4.50 (m, 1H, 18H), 4.49−4.26 (m, 2H, OCH_2Ar), 4.20−4.00 (m, 1H, 17H), 3.46 (q, J = 8.0, 2H, 8-CH_2CH_3), 3.35−2.99 (m, all 3H, for 3 × ring CH_3), 2.40−2.73, 2.38−2.18 (m, 4H, 17^1- and 17^2-H), 2.08 (s, 3H, 3^2-CH_3), 1.61 (d, J = 7.6, 3H, 18-CH_3), 1.48 (s, 3H, 8-CH_2CH_3), 0.07 (brs, 1H, NH), −1.82 (brs, 1H, NH). ^{13}C NMR ($CDCl_3$; 400 MHz): δ 196.95, 171.71, 160.67, 155.35, 151.04, 149.13, 145.13, 141.38, 140.87, 138.51, 137.85, 137.11, 136.91, 135.4, 132.99, 130.34, 128.41, 127.94, 127.35, 106.16, 104.13, 97.93, 94.62, 93.00, 72.19, 70.37, 51.74, 50.19, 48.14, 31.24, 29.97, 24.73, 23.29, 19.58, 17.59, 14.21, 12.03, 11.53, 11.26, 1.25. MS for $C_{40}H_{41}N_4O_4I$: 768.22 (calcd), 769.2 (found, MH^+). Anal. Calcd for $C_{40}H_{41}N_4O_4I$: C, 62.50; H, 5.38; N, 7.29. Found: C, 62.59; H, 5.42; N, 7.20.

Synthesis of 3-Devinyl-3-{1′-(*m*-trimethylstannylbenzyloxy)ethyl}pyropheophoride-*a* (5). To the solution of methyl 3-devinyl-3-{1′-(*m*-iodobenzyoxy)ethyl}pyropheophoride-*a* carboxylic acid (**4**) (50 mg, 0.065 mmol) in dry THF were added hexamethydistannane (0.1 mL, 0.48 mmol) and bis(triphenylphosphine) palladium(II)dichloride (10 mg, 0.014 mmol), and the reaction mixture was stirred at room temperature for overnight. The solvent was evaporated. The crude product was purified by preparative plates. 4% methanol/dichloromethane was used as the eluting solvent to yield compound **5**. The compound obtained after evaporating the solvents was crystallized from dichloromethane/hexane in 75% yield (39 mg). mp >320 °C .UV−visible, λ_{max} (MeOH/CH_2Cl_2), nm (ε): 663 (4.65×10^4), 606 (9.20×10^3), 537 (9.42×10^3), 506 (9.64×10^3), 411 (9.52×10^4). ^1H NMR ($CDCl_3$; 400 MHz): δ 9.74, 9.50, and 8.53 (all s, 1H, meso-H), 7.50 (m, 2H, ArH), 7.40 (m, 2H, ArH), 6.01 (q, J = 6.4, 1H, 3^1-H), 5.27 (d, J = 17.6, 1H, 13^2-CH_2), 5.10 (d, J = 19.6, 1H, 13^2-CH_2), 4.78 (dd, J = 5.4, 11.9, 1H, OCH_2Ar), 4.60 (dd, J = 1.7, 12.0, 1H, OCH_2Ar), 4.50 (m, 1H, 18-H), 4.28 (m, 1H, 17-H), 3.70 (q, J = 7.8, 2H, 8-CH_2CH_3), 3.64, 3.35, and 3.16 (m, all 3H, for 3 × ring CH_3), 2.36−2.76, 2.50−2.62, and 2.20−2.34 (m, 4H, 17^1- and 17^2-H), 2.14 (m, 3H, 3^2-CH_3), 1.81 (d, J = 5.6, 3H, 18-CH_3), 1.71 (t, J = 7.6, 3H, 8-CH_2CH_3), 0.50 (br s, 1H, NH), 0.19 (s, 9H, *tert*-butyltin), −1.70 (br s, 1H, NH). ^{13}C NMR ($CDCl_3$; 400 MHz): δ 197.39, 172.07, 160.96, 155.59, 151.08, 149.12, 145.21, 141.32, 140.68, 138.46, 137.63, 137.03, 136.49, 135.49, 133.11, 130.21, 130.01, 128.37, 127.80, 127.29, 114.66, 105.88, 104.21, 97.77, 94.44, 93.00, 72.08, 70.30, 51.72, 50.21, 48.03, 31.47, 31.11, 30.32, 29.75, 24.52, 23.14, 19.49, 17.44, 14.24, 11.95, 11.33, 11.09, 1.05. Mass: calcd for $C_{43}H_{50}N_4O_4Sn$, 806.3; found, 807.5 (MH^+). HRMS: calcd for $C_{43}H_{51}N_4O_4Sn$ (MH), 807.2932; found, 807.2995.

Synthesis of Peglate 3-Devinyl-3-{1′-(*m*-iodobenzyoxy)ethyl}pyropheophoride-*a* (7). Methyl 3-devinyl-3-{1′-(*m*-iodobenzyoxy)ethyl}pyropheophoride-*a* carboxylic acid (**4**) (50 mg, 0.065 mmol), PEG (390 mg, 0.078 mmol), DCCI (13.8 mg, 0.072 mmol), and DMAP (7.93 mg, 0.065 mmol) were dissolved in anhydrous DMF (4 mL). The reaction mixture was stirred at room temperature for overnight. The solvent was evaporated. The crude product was purified by preparative plates. 4% methanol/dichloromethane was used as the eluting solvent to yield compound **7**. It was then crystallized from dichloromethane/hexane in 51% yield (191 mg). mp >320 °C. UV−visible, λ_{max} (CH_2Cl_2), nm (ε): 664 (4.64×10^4), 607 (9.22×10^3), 535 (9.43×10^3), 507 (9.66×10^3), 412 (9.53×10^4). ^1H NMR ($CDCl_3$; 400 MHz): δ 9.77, 9.76 (two s, 1H, 5-H), 9.54, and 8.59 (each s for 1H, 5- and 10-*meso*-H), 7.75, 7.63, 7.07, 6.89 (each m for 1H, ArH), 7.40 (m, 2H, ArH), 5.96 (q, J = 6.3, 1H, 3^1-H), 5.28 (d, J = 17.7, 1H, 13^2-CH_2), 5.12 (d, J = 17.6, 1H, 13^2-CH_2), 4.68 (dd, J = 5.4, 11.3, 1H, OCH_2Ar), 4.57 (m, 2H, 1H for OCH_2Ar, 1H for 17-H), 4.35 (m, 1H, 18-H), 4.04−3.14 (broad and high peak, many protons, including all protons from PEG group $-NHCH_2CH_2(OCH_2CH_2)_nOCH_3$, another 11H for 2-$CH_3$, 7-$CH_3$, 12-$CH_3$, and 8-$CH_2CH_3$), 2.43 (m, 2H, 17^1-H), 2.17 (m, 2H, 17^2-H), 1.82 (d, J = 5.5, 3H, 3-CH_3), 1.70 (t, J = 7.6, 3H, 18-CH_2CH_3), 1.25 (brs, 1H, NH), −1.73 (brs, 1H, NH). HRMS: calcd for $C_{267}H_{496}N_5O_{116}I$, 5756.2111; found, 5756.2132.

Synthesis of Methyl 3-Devinyl-8-{1′-(*m*-iodobenzyoxy)ethyl}pyropheophoride-*a* (11). Methyl 3-devinyl-3-ethyl-7,8-dihydroxypyropheophoride-*a* (**10**) (100 mg, 0.17 mmol) was reacted with 3-iodobenzyl alcohol in refluxing toluene, and a few drops of HCl was added. The reaction mixture was neutralized with $NaHCO_3$ in H_2O, and compound was extracted with CH_2Cl_2. The organic layer was washed with H_2O and dried over Na_2SO_4. The crude product was purified by preparative plates, using 5% methanol/dichloromethane as the eluting solvent. Two bands were separated and identified as follows: the slower moving band (minor product) was characterized as methyl 3-devinyl-3-ethyl-8-vinyl pyropheophoride-*a* (**16**); the faster moving band (major product, 54 mg, 40% yield) was identified as the desired product **11**, mp: 130−132 °C. UV−visible, λ_{max} (CH_2Cl_2), nm (ε): 656 (4.69×10^4), 599 (8.22×10^3), 539 (8.14×10^3), 506 (9.91×10^3). ^1H NMR ($CDCl_3$; 400 MHz): δ 9.98, 9.26, 8.48 (all s, 1H, meso-H), 7.71 (d, J = 4.0, 1H, ArH), 7.59 (d, J = 8.0, 1H, ArH), 7.20 (t, J = 8.2, 1H, ArH), 7.05 (t, J = 8.2, 1H, ArH), 5.78 (q, 6.8, 1H, 8^1-H), 5.28 (d, J = 19.8, 1H, 13^2-CH_2), 5.13 (d, J = 19.8, 1H, 13^2-CH_2), 4.68 (d, J = 13.0, 1H, OCH_2Ar), 4.56 (d, J = 11.6, 1H, OCH_2Ar), 4.41−4.48 (m, 1H, 18-H), 4.22−4.31 (m, 1H, 17-H), 3.84 (q, J = 8.0, 2H, 3-CH_2CH_3), 3.62, 3.59, 3.30, and 3.28 (all s, all 3H, for 17^3-$COOCH_3$ and 3 × ring CH_3), 2.61−2.75, 2.44−2.58, and 2.17−2.35 (m, 4H, 17^1- and 17^2-H), 2.12 (t, J = 4.8, 3H, 8^2-CH_3), 1.79 (t, J = 10.4, 3H, 18-CH_3), 1.73 (t, J = 7.6, 3H, 3-CH_2-CH_3), 0.41 (brs, 1H, NH), −1.74 (brs, 1H, NH). ^{13}C NMR ($CDCl_3$; 400 MHz): δ 196.42, 173.69, 172.16, 160.78, 153.90, 149.58, 148.86, 142.67, 142.19, 141.33, 138.03, 137.24, 136.83, 131.44, 130.68, 129.55, 128.08, 127.38, 119.98, 114.96, 106.67, 105.97, 96.22, 94.65, 92.77, 72.55, 70.20, 51.90, 50.24, 48.22, 31.11, 30.08, 25.39, 23.32, 19.61, 18.70, 17.17, 12.72, 12.41, 11.61, 11.17. MS for $C_{41}H_{43}O_4N_4I$: 782.23 (calcd), 805.1 (found, M + 23). Anal. Calcd for $C_{41}H_{43}O_4N_4I$: C, 62.90; H, 5.54; N, 7.16. Found: C, 62.80; H, 5.52; N, 7.11.

Synthesis of 3-Devinyl-3-ethyl-8-{1′-(*m*-iodobenzyoxy)ethyl} pyropheophoride-*a* (12). Methyl 3-devinyl-8-{1′-(*m*-iodobenzyoxy)ethyl}pyropheophoride-*a* (**11**) was reacted with aqueous LiOH by following the method discussed for the preparation of 3-devinyl-3-{1′-(*m*-iodobenzyoxy)ethyl}pyropheophoride-*a* carboxylic acid (**4**), and **12** was obtained in 70% yield, mp: 171−172 °C. UV−visible, λ_{max} (CH_2Cl_2), nm (ε): 655 (4.65×10^4), 600 (8.03×10^3), 538 (8.00×10^3), 506 (9.63×10^3). ^{1}H NMR ($CDCl_3$; 400 MHz): δ 9.90, 9.16, and 8.42 (all s, 1H, meso-H), 7.70 (s, 1H, ArH), 7.55 (d, J = 7.8, 1H, ArH), 7.21 (d, J = 8.0, 1H, ArH), 6.962 (t, J = 8.0, 1H, ArH), 5.73 (q, J = 8.0, 1H, 8^1-H), 4.95−5.36 (m, 2H, 13^2-CH_2), 4.57−4.70 (m, 1H, 18H), 4.44−4.54 (d, J = 10.4, 1H, OCH_2Ar), 4.43−4.33 (m, 1H, OCH_2Ar), 4.20−4.24 (m, 1H, 17H), 3.75 (q, J = 8.0, 2H, $-CH_2CH_3$), 3.56, 3.25, 3.22 (all s, all 3H, for 3 × ring CH_3), 2.47−2.71, 2.20−2.37 (m, 4H, 17^1 and 17^2-H), 2.09 (s, 3H, 8^2-CH_3), 1.78 (s, 3H, 18-CH_3), 1.67 (s, 3H, 3-CH_2CH_3), 0.85 (brs, 1H, NH), −1.72 (brs, 1H, NH). ^{13}C NMR ($CDCl_3$; 400 MHz): δ 197.25, 173.94, 172.50, 160.65, 154.17, 149.36, 148.67, 142.64, 142.01, 140.84, 138.01, 137.28, 137.02, 136.86, 136.60, 131.53, 130.05, 129.80, 129.12, 127.61, 127.22, 114.49, 105.38, 95.81, 94.19, 92.62, 72.27, 69.94, 51.59, 51.42, 50.01, 30.79, 29.79, 29.57, 24.87, 22.85, 19.23, 16.71, 11.89, 11.16 . Mass for $C_{40}H_{41}O_4N_4I$: 768.22 (calcd), 769.4 (found, MH^+). Anal. Calcd for $C_{40}H_{41}O_4N_4I$: C, 62.50; H, 5.38; N, 7.29. Found: C, 62.39; H, 5.45; N, 7.20.

Synthesis of Methyl 3-(1′-(3-Iodobenzyloxy)ethyl)-3-deacetylbacteriopyropheophorbide-*a* (19). Compound **18**[29] (100.0 mg, 0.17 mmol, 1.0 equiv) was dissolved in dry CH_2Cl_2 (15 mL), and HBr gas was bubbled into the solution for 2 min. The reaction mixture was stirred for 5 min at room temperature. The solvent was evaporated under high vacuum, the resulting crude was dried, and the entire crude was dissolved in dry CH_2Cl_2 (15 mL). A 50.0 mg portion of dry K_2CO_3 was added to this mixture, followed by addition of 3-iodobenzyl alcohol (0.25 mL). The resulting reaction mixture was stirred for 30 min at room temperature and then worked up. Purification of the crude mixture was done by column chromatography (silica gel, 50% ethyl acetate in hexanes). Yield: 89 mg, 65%. ^{1}H NMR (400 MHz, $CDCl_3$): δ 8.52/8.53, 8.23, 8.04 (all s, 1H, meso-H), 7.72 (d, 1H, ArH), 7.62 (d, J = 8.0 Hz, 1H, ArH), 7.25 (s, 1H, ArH), 7.04 (t, 1H, ArH), 5.68−5.73 (m, 1H, 3^1-H), 4.96 (d, J = 19.6 Hz, 1H, 13^1-H), 4.79 (d, J = 19.6 Hz, 1H, 13^1-H), 4.60−4.63 (m, 1H, OCH_2Ar), 4.45−4.50 (m, 1H, OCH_2Ar), 4.14−4.19 (m, 2H, 7-H + 18-H), 4.00−4.02 (m, 1H, 17-H), 3.88−3.90 (m, 1H, 8-H), 3.61 (s, 3H, $COOCH_3$), 3.35 (s, 3H, 12-CH_3), 3.14 (s, 3H, 2-CH_3), 2.44−2.59 (m, 2H, 8^1-H + 17^1-H), 2.21−2.43 (m, 4H, 17^1-H + 17^1-CH_2 + 8^1-H), 2.01 (d, J = 8.0 Hz, 3H, 3^1-CH_3), 1.65−1.77 (doublets, 6H, 18-CH_3 + 7-CH_3), 1.12 (t, 3H, 8^1-CH_3). ^{13}C NMR ($CDCl_3$; 400 MHz): δ 195.56, 173.54, 170.95, 170.85, 170.21, 161.53, 155.22, 147.83, 147.81, 140.78, 140.74, 140.70, 140.62, 138.48, 138.41, 137.37, 137.36, 136.95, 136.84, 136.74, 136.02, 135.99, 133.67, 130.12, 127.13, 127.09, 118.22, 118.18, 108.74, 99.24, 99.21, 95.00, 94.94, 94.35, 93.82, 93.80, 71.72, 71.49, 70.10, 70.00, 54.34, 54.30, 51.65, 50.43, 50.41, 49.89, 49.06, 47.38, 30.78, 30.21, 30.19, 29.88, 24.01, 23.90, 22.78, 22.63, 22.54, 22.51, 11.26, 10.88, 10.84, 10.80. MS (ESI): m/z 785.4 (M + H^+). HRMS (ESI): calcd for $C_{41}H_{46}IN_4O_4$, 785.2564; found, 785.2587 (MH^+). UV−vis (CH_2Cl_2, λ_{max}, nm, (ε)): 719 (3.58×10^4), 659 (1.21×10^4), 602 (4.71×10^3), 517 (2.55×10^4), 486 (6.69×10^3), 456 (2.81×10^3), 382 (4.59×10^4), 354 (8.63×10^4).

Synthesis of Methyl-3-deacetyl-3-(1′-*m*-iodobenzyloxyethyl)-7,8-dihydrophylloerythrin (20). Compound **19** (50.0 mg, 0.06 mmol, 1.0 equiv) was dissolved in dichloromethane (50 mL). To this mixture was added slowly a nitromethane (4 mL) solution of $FeCl_3 \cdot 6H_2O$ (68.9 mg, 0.25 mmol, 4.0 equiv). The resulting reaction mixture was stirred at room temperature for 30 min, quenched by addition of 20 mL of methanol, and washed with water three times. The organic layer was separated and dried over anhydrous Na_2SO_4, and solvent was removed under vacuum. The product obtained after evaporating the solvents was purified by preparative plates (silica gel; eluting solvent, 2% acetone in dichloromethane). Yield: 35.0 mg, 70%. UV−vis (CH_2Cl_2, λ_{max}, nm, (ε)): 670 (4.69×10^4), 613 (5.54×10^3), 540 (5.11×10^3), 513 (9.57×10^3), 413 (7.70×10^4). ^{1}H NMR (400 MHz, CDCl3): δ 9.21, 9.00/8.99, 8.65 (all s, 1H, meso-H), 7.75 (d, 1H, ArH), 7.62 (d, J = 8.0 Hz, 1H, ArH), 7.25 (s, 1H, ArH), 7.04 (t, J = 8.0 Hz, 1H, ArH), 5.91 (m, 1H, 3^1-H), 5.44 (s, 2H, 13^1-H), 4.64−4.67 and 4.50−4.54 (m, 2H, OCH_2Ar), 4.43−4.45 and 4.21 (m, 2H, 7-H + 8-H), 3.83 (t, J = 8.0 Hz, 2H, 17^1-CH_2), 3.74 (s, 3H, $COOCH_3$), 3.55 (s, 3H, 12-CH_3), 3.42 (s, 3H, 2-CH_3), 3.21 (s, 3H, 18-CH_3), 2.91 (t, J = 8.0 Hz, 2H, 17^2-CH_2), 2.44−2.49 (m, 1H, 8^1-H), 2.14−2.17 (m, 4H, 8^1-H + 3^1-CH_3), 1.80/1.90 (distorted d, 3H, 7-CH_3), 1.16 (t, 3H, 8^1-CH_3). ^{13}C NMR ($CDCl_3$; 400 MHz): δ 195.99, 195.98, 173.11, 172.15, 172.06, 166.25, 154.24, 146.54, 145.24, 145.22, 142.43, 140.79, 140.69, 139.77, 139.61, 139.31, 137.31, 136.98, 136.87, 136.75, 136.38, 136.31, 135.19, 135.13, 133.54, 130.12, 127.19, 127.12, 121.73, 121.72, 115.51, 97.08, 97.05, 96.72, 96.68, 94.49, 94.38, 93.85, 93.77, 71.97, 71.71, 70.18, 70.06, 55.55, 55.51, 51.82, 51.81, 48.96, 48.95, 48.90, 36.08, 30.35, 30.30, 24.34, 24.19, 23.36, 23.23, 11.66, 11.64, 11.22, 11.19, 11.18, 11.17, 11.04, 11.00. MS (ESI): m/z 783.4 (M + H^+). HRMS (ESI): calcd for $C_{41}H_{44}IN_4O_4$, 783.2407; found, 783.2410 (MH^+). Anal. Calcd for $C_{41}H_{43}IN_4O_4$: C, 62.91; H, 5.54; N, 7.16. Found: C, 62.85; H, 5.57; N, 7.01.

Synthesis of 3-Deacetyl-3-(1′-*m*-iodobenzyloxyethyl)-7,8-dihydrophylloerythrin (23). Compound **20** (40 mg, 0.05 mol, 1equiv) was dissolved in degassed THF (10 mL). Degassed water and a solution of $LiOH \cdot H_2O$ (50 mg, 1.19 mmol, 23 equiv) in methanol (10 mL, 1:1 v/v) were added. The entire reaction mixture was then stirred under nitrogen atmosphere at room temperature for 2 h, and the resulting mixture was diluted with dichloromethane (20 mL). It was then washed with water (3 × 200 mL). The organic layer was separated and dried over Na_2SO_4, and the solvent was removed under reduced pressure. The residue obtained was purified by preparative TLC (silica gel, 5% methanol in CH_2Cl_2) and crystallized from dichloromethane/hexane. Yield: 22 mg, 55%. UV−vis (CH_2Cl_2, λ_{max}, nm, (ε)): 670 (4.69×10^4), 613 (5.54×10^3), 540 (5.11×10^3), 513 (9.57×10^3), 413 (7.70×10^4). ^{1}H NMR (400 MHz, $CDCl_3$): δ 9.21, 8.64 (all s, 1H, meso-H), 7.73 (d, 1H, ArH), 7.60 (d, 1H, ArH), 7.24 (s, 1H, ArH), 6.99−7.05 (m, 1H, ArH), 5.87−5.88 (m, 1H, 3^1-H), 5.40 (s, 2H, 13^1-H), 4.48−4.62 and 4.48−4.53 (m, 2H, OCH_2Ar), 4.40−4.43 and 4.19−4.21 (m, 2H, 7-H + 8-H), 3.86 (m, 2H, 17^2-CH_2), 3.53 (s, 3H, 12-CH_3), 3.30 (s, 3H, 2-CH_3), 3.22 (s, 3H, 18-CH_3), 2.95 (t, 2H, 17^1-CH_2), 2.43−2.47 (m, 1H, 8^1-H), 2.12−2.17 (m, 4H, 8^1-H + 3^1-CH_3), 1.75−1.89 (d, 3H, 7-CH_3), 1.13 (m, 3H, 8^1-CH_3). MS(ESI): m/z 769.2 (M + H^+). HRMS (ESI): calcd for $C_{40}H_{42}IN_4O_4$, 769.2251; found, 769.2271 (MH^+).

Synthesis of Methyl 3-{1′-(*m*-Trimethylstannylbenzyloxy) ethyl}-7,8-dihydrophylloerythrin (25). To a solution of **20** (50 mg, 0.06 mmol, 1.0 equiv) in dry DMF (10 mL) were added hexamethylditin (83 mg, 0.25 mmol, 4.0 equiv) and $Pd_2(dba)_3 \cdot CHCl_3$ (6.6 mg, 0.006 mmol, 0.1 equiv), and the reaction mixture was stirred at 50 °C for 4 h. After removal of the solvent under vacuum to dryness, the crude mixture was purified by preparative plates using 5% acetone/CH_2Cl_2 to give **25**. Yield = 21 mg, 40% UV−vis (CH_2Cl_2, λ_{max}, nm, (ε)): 669, 613, 540, 513, 413. ^{1}H NMR (400 MHz, $CDCl_3$): δ 9.17, 9.06, 8.65 (all s, 1H, meso-H), 7.26−7.51 (m, 4H, ArH), 5.92−5.97 (m, 1H, 3^1-H), 5.53 (s, 2H, 13^1-H), 4.69−4.77 and 4.56−4.62 (m, 2H, OCH_2Ar), 4.42−4.45 and 4.22 (m, 2H, 7-H + 8-H), 3.75 (overlapped, 5H, 2H of 17^1-CH_2, 3H of $COOCH_3$), 3.56 (s, 3H, 12-CH_3), 3.42 (s, 3H, 2-CH_3), 3.18 (s, 3H, 18-CH_3), 2.88 (t, J = 8.0 Hz, 2H, 17^2-CH_2), 2.51 (m, 1H, 8^1-H), 2.14−2.17 (m, 4H, 8^1-H + 3^1-CH_3), 1.80/1.89 (d, J = 8.0 Hz, 3H, 7-CH_3), 1.16 (t, 3H, 8^1-CH_3), 0.25 (s, 9H, $Sn(CH_3)_3$). ^{13}C NMR ($CDCl_3$; 400 MHz): δ 196.05, 173.14, 172.24, 172.13, 166.18, 154.37, 146.55, 145.26, 142.56, 142.46, 142.34, 139.84, 139.79, 139.35, 137.68, 137.62, 137.46, 136.35, 136.24, 135.72, 135.62, 135.53, 135.50, 135.26, 135.19, 133.51, 128.25, 128.19, 128.17, 128.04, 121.60, 115.50, 96.96, 96.92, 96.72, 96.66, 94.02, 93.86, 71.74, 71.39, 71.28, 71.23, 55.55, 55.46, 51.81, 48.94, 36.12, 30.36, 30.30, 24.43, 24.20, 23.33, 23.19, 22.44, 11.64, 11.24, 11.19, 11.15, 10.96, 10.92, −9.58,

−9.59. MS (ESI): m/z 821.5 (M + H^+). HRMS (ESI): calcd for $C_{44}H_{52}N_4O_4Sn$, 821.3089; found, 821.3078 (MH^+).

3-Deacetyl-3-(1′-*m*-trimethylstannylbenzyloxyethyl)-7,8-dihydrophylloerythrin (24). To a solution of **23** (9.0 mg, 0.01 mmol, 1.0 equiv) in dry THF was added hexamethydistannane (35.0 μL) and bis(triphenylphosphine)palladium(II)dichloride (3.2 mg, 0.004 mmol, 0.4 equiv), and the reaction mixture was stirred at room temperature for overnight. The solvent was evaporated. The crude product was purified by preparative plates. 4% methanol/dichloromethane was used as the eluting solvent to yield compound (**24**). Yield: 6.0 mg (75%), UV−visible, $\lambda_{max}(CH_2Cl_2)$, nm (ε): 670, 613, 541, 513, 412. ^{1}H NMR ((C_4D_8)O); 400 MHz): δ 9.23, 9.11/9.03, 8.70 (all s, 1H, meso-H), 7.48 (d, 1H, ArH, J = 7.6 Hz), 7.39−7.34 (m, 2H, ArH), 7.32−7.23 (m, 1H, ArH), 6.03−5.98 (m, 1H, 3^1-H), 5.25 (s, 2H, 13^1-H), 4.60−4.72 (m, 2H, OCH_2Ar), 4.42−4.45 and 4.17−4.18 (broad m, 2H, 7-H + 8-H), 3.68 (broad m, 2H, 17^2-CH_2), 3.47 (s, 3H, 12-CH_3), 3.40 (s, 3H, 2-CH_3), 3.15 (s, 3H, 18-CH_3), 2.83 (t, 2H, 17^1-CH_2, J = 8.0 Hz), 2.68 (broad m, 5H, 2H of 8^1-H + 3H of 3^1-CH_3), 2.11/2.12 (distorted D, 3H, 7-CH_3), 1.18 (m, 3H, 8^1-CH_3), 0.20 and 0.18 (splitted s, 9H, Sn(CH_3)$_3$). MS(ESI): m/z 807.3 (M + H^+). HRMS (ESI): calcd for $C_{43}H_{51}N_4O_4Sn$ (MH), 807.2932; found, 807.2920.

General Method for the Preparation of ^{124}I-Labeled Photosensitizers 6, 26, and 27. The trimethyltin analogue (**5**, **25**, or **24**, respectively) (60 μg) dissolved in 5% acetic acid in methanol (50 μL) was added to a tube containing dried Na^{124}I (60 ng). To this solution was added 10 μL of *N*-chlorosuccinimide (1 mg/mL in methanol). The reaction mixture was incubated at room temperature for 8 min. The reaction mixture was loaded onto a HPLC column (symmetry C18 5 μm, 4.6 mm × 150 mm). A mixture of methanol/water (88:12) was used as eluant. The flow rate was 1 mL/min. The UV detector was set at 254 nm. The labeled product was collected, and the solution was evaporated under nitrogen gas flow at 80 °C. The product was dissolved in 10% ethanol/saline solution for in vivo experiments. The radiochemical yield was 30%, and the specific activity was greater than 1 Ci/μmol. The purity was ascertained by HPLC.

HPLC Analyses of the Final Products. HPLC analyses of compounds **4**, **12**, and **23** were performed using a Waters Delta 600 System consisting of the 600 Controller, 600 Fluid Handling Unit, and 996 photodiode array detector equipped with a EMD LichroCart RP8, reverse phase C8 column, 5 μm particle size with dimensions of 4 mm × 250 mm . Compounds were eluted at a flow rate of 1.5 mL/min using a gradient program: solvent A, methanol; solvent B, water; gradient profile: 0 min, 75% A/25% B; linear grade to 90% A/10% B from 0 to 10 min; maintained at this composition until 20 min; then linear grade to 100% A. The retention time and percent purity of each compound were as follows: **4**, 10.13 min; **12**, 10.48 min; and **23**, 9.94 min. The component percentages are based on the area counts of the peaks from the 408 nm channel.

Cell Cultures. A subclonal line of human basal cell carcinoma cells (Dicker et al., 2002, J. Invest Dermatol 118: 859-865) (provided by Dr. Tak-Wah Wang) were cultured in DMEM containing 10% fetal calf serum. PS uptake was determined in subconfluent cultures established in 24- or 6-well culture plates. The cells were washed twice with serum-free DMEM, and cells and then incubated in DMEM containing the concentration of fetal calf serum and photosensitizers as indicated in the specific experiments. After an incubation period ranging from 30 to 24 h, the cells were washed with serum-free DMEM. Cell-associated PS was visualized by 640× fluorescent microscopy on an inverted fluorescence microscope (Zeiss Axiovert 200) with an Axio camera. The filters for HPPH fluorescence were Ex 410/40 nm and Em 675/750 nm. Internalization of PS was achieved by incubating PS-treated cells in serum-free or serum-containing medium for 4−24 h at 37°. PS amounts in cells were quantified by extraction in Solvable (PerkinElmer Life and Analytical Sciences) and measurement of fluorescence (Ex 415 nm; Em 667 nm) in a Varian Cary Eclipse fluorescence spectrophotometer (Agilent Technologies, Santa Clara, CA).

Photoreaction was performed by illuminating PS-treated cell cultures in serum-free medium at 37 °C (within a tissue culture incubator) with 665 nm light of an argon-pumped dye laser for 9 min to a total fluence of 3 J/cm^2. Depending upon the experimental design, cells were either extracted immediately after light treatment (identification of signaling reaction) or incubated at 37 °C for 24 h (evaluation of PDT-mediated cell kill).

Cell Analyses. Survival was defined as the percent viable cells recovered after 24 h of PDT and incubation in full growth medium. Cells were released by trypsin treatment, and trypan blue-excluding cells were counted in a hemocytometer. For protein analysis, cells were lysed in radioimmunoprecipitation assay (RIPA) buffer and subjected to protein analyses as described.[8,9] Briefly, protein extracts (20 μg) were separated on 6% to 10% SDS-polyacrylamide gels. On all gels, reference protein markers for loading, molecular size detection, and cross-comparison among gels were included. After separation, proteins were transferred to Hybond-P membranes (Amersham Pharmacia Biotech). Nonspecific interactions were blocked by incubating the membranes with PBS-0.1% Tween 20−5% skim milk. Membranes were then reacted overnight at 4 °C with one of the primary antibodies: STAT3 (Santa Cruz Biotechnology, Santa Cruz, CA), p38 P-p38, and EGFR (Cell Signaling Technologies, Inc., Danver, MA). The immune complexes were visualized by reacting with peroxidase-coupled secondary antibodies and enhanced chemiluminescence detection (ECL) (Pierce Chemicals, Rockford, IL). ECL images were recorded on X-ray films by various lengths of exposure to ensure recovery of signals within the linear range of digital scanning. The net pixel values of each band were integrated by using the ImageQuant TL program (Amersham Biosciences). The cross-comparison of separate analyses and immunoblots relied on coseparated reference markers. STAT3 cross-linking was expressed by the percent conversion of monomeric STAT3 into the dimer form I of the STAT3 cross-linked complexes.[31]

To quantify the uptake of PS by Colon26 cells, the cells were seeded in six-well plates with 0.33 × 10^6 cells per well in 2 mL of growth medium. The cells were incubated overnight at 37 °C. Four concentrations (100, 200, 400, and 800 nM) of the photosensitizers were added to triplicate wells and incubated at 37 °C for 4 h. Triplicate wells without photosensitizers were included to determine the baseline autofluorescence. The cells were then harvested by trypsinization, neutralized with cold medium containing 2% FCS, transferred to 5 mL flow cytometry tubes and centrifuged for 5 min at 500 g at 4 °C to prevent efflux of the photosensitizers. The supernatant was removed, the cell pellet resuspended with 0.25 mL cold PBS containing 2% FCS, placed on ice in the dark and immediately analyzed by flow cytometry. Data was acquired with Cell Quest on an LSRII flow cytometer (Beckton and Dickenson), using an excitation wavelength of 633 nm and detecting fluorescence emission at 730± 45 nm of 10,000 events and analyzed with FCS Express (Denovo software). Histograms were generated and data was expressed as the mean fluorescence of triplicate samples after subtracting autofluorescence.

The photosensitizing activity was determined in Colon26 cells using the colorimetric MTT assay. Colon26 cells were seeded in 96-well plates at a density of 3 × 10^3 cells/well in RPMI with 10% fetal calf serum. After overnight incubation, the PSs were added at the indicated concentrations and incubated at 37 °C for 24 h in the dark. Before light treatment, the medium was replaced with drug-free complete medium. Cells were then illuminated (0−4 J/cm^2) with 665 nm for compounds **1**, **4**, and **7**, using 660 nm light for compound **12** and 674 nm for compound **23** from an argon-pumped dye laser at a fluence rate of 3.2 mW/cm^2. After PDT, the cells were incubated for a further 48 h at 37 °C in the dark. During the last 4 h of incubation, 10 μL of a 4.0 mg/mL solution in PBS of 3-[4,5-dimethylthiazol-2-yl]-2,5-diphenyltetrazoliumbromi (MTT) (Sigma, St. Louis, MO) was added to each well. After 4 h, the MTT and medium were removed and 100 μL of DMSO was added to solubilize the formazan crystals. Absorbances were read on a microtiter plate reader

(BioTek Instruments, Inc., ELx800 Absorbance Microplate Reader) at 570 nm. The results were plotted as the survival rate of treated cells against different light doses for each compound tested. Each experiment was done with four replicate wells and repeated three times independently to obtain an accurate photosensitizing efficacy.

Animal Models. The photosensitizers were evaluated in mice (BALB/c, 10 mice/group) bearing Colon26 tumors, implanted subcutaneously, and were allowed to grow to an approximate diameter of 5−7 mm. All animal procedures were carried out in accordance with guidelines approved by the Institute Animal Use and Care Committee.

PET Imaging. Mice were imaged in the micropet FOCUS 120, a dedicated 3D small-animal PET scanner (Concorde Microsystems Inc.) at State University of New York at Buffalo (South Campus) under the Institutional Animal Care and Use Committee (IACUC) guidelines. All BALB/c mice (n = 10 for each compound) tumored with Colon26 cells were injected via the tail vein with 52−122 μCi of PS **1**, **6**, and **27**, respectively. After 24, 48, and 72 h postinjection, the mice were anesthetized by inhalation of isoflurane/oxygen and placed head first, prone for imaging, and the acquisition time was set for 30 min. No efforts were made to block the radioiodine uptake by thyroid or stomach, and surprisingly, in only a few cases was a little bit of radioiodine uptake observed in the thyroid, and that too was cleared by 72 h. Some tumored mice were also imaged using ^{18}F-FDG radiotracer 24 h prior to radioactive ^{124}I imaging. These mice were administered 150−200 μCi of ^{18}F-FDG via the tail vein and were scanned for 20 min in the fashion described above, beginning 45 min after FDG injection. For biodistribution studies, the mice were injected with 15−50 μCi of compounds PS **1**, **6**, and **27**, respectively, via the tail vein, and three mice each at 24, 48, and 72 h time interval were sacrificed, and body organs (tumor, heart, liver, spleen, kidney, lung, muscle, etc.) were removed immediately. After weighing, the amount of radioactivity in the tumor (300−400 mg), body organs, and blood was measured by a γ-well counter. Radioactivity uptake was calculated as the percentage of the injected dose per gram of the tissue (%ID/g). Statistical analyses and data (%ID/g vs time point) were plotted using GraphPad Prism 5.

In Vivo PDT Efficacy and the Assessment of Response. Before PDT treatment, Nair was used to remove all hair surrounding the tumor site. When the tumor reached 4−5 mm in diameter, the mice were injected with compounds **1**, **4**, 7, **12**, and **23** at a dose of 1 μmol/kg. At 24 h postinjection, the mice were restrained in plastic Plexiglass holders without anesthesia and treated with laser light (665 nm for compounds **1**, **4**, and **7**; 660 nm for compound **12**, and 674 for compound **23**, 128 J/cm^2, 14 mW/cm^2). The power was monitored during the entire treatment. Post-PDT, the mice were observed daily for tumor regrowth or tumor cure. Visible tumors were measured using two orthogonal measurements L and W (perpendicular to L), and the volumes were calculated using the Microsoft Excel formula $V = LW^2/2$ and recorded. Mice were considered cured if there was no palpable tumor by day 60−90. Once the tumor reached 400 mm^3, the mice were euthanized due to tumor burden as per RPCI IACUC rules.

In Vivo Optical Fluorescence Imaging. In vivo fluorescence imaging was accomplished by using a Illumination Dual Light System (Lightools Research, Encinitas, CA), designed for small animal studies. True-Color fluorescence images were obtained using dielectric long-pass filters (Chroma Tech) and a digital color camera (Optronics, Magnafire SP, Olympus America). Wavelength-resolved spectral imaging was carried out by using a Nuance multispectral imaging system (CRI, Inc., Woburn, MA) comprising an optical head that includes Varispec liquid crystal tunable filters (LCTFs, with a bandwidth of 20 nm and a scanning wavelength range of 400−720 nm), an optical coupler, and a high-resolution scientific-grade CCD camera, along with image acquisition and analysis software. The tunable filter was automatically stepped in 10-nm increments from 550 to 720 nm while the camera captured images at each wavelength with a constant exposure. The 27 resulting TIFF images were loaded into a single data structure in memory, forming a spectral stack with a spectrum at every pixel. Autofluorescence spectra and PS fluorescence spectra were manually selected from the spectral image using the computer mouse to select appropriate regions. Spectral unmixing algorithms (available from CRI, Inc.) were applied to create the unmixed images of pure autofluorescence and pure PS fluorescence signals, as shown in Figure 11 and 12. All the images were reanalyzed using Image J software to show false color fluorescence reflectance (FRI) images.

Following an IACUC-approved protocol, the BALB/c mice were subcutaneously injected with 1 × 10^6 Colon26 cells in 50 μL of serum free complete RPMI-1640 media (into the right posterior axilla), and tumors were grown until they reached 4−5 mm in diameter. The day before PS injection, all hairs were removed from the inoculation site and the mice were imaged under anesthesia (IP injection of ketamine and xylazine mixture). In a dark box, illumination was provided by fiber optic lighting at 540/40× nm (green color), and a long-pass filter was used to reject scattering and to pass Stoke-shifted PS fluorescence at 667 nm and 676 nm, respectively. Under similar conditions, mice were imaged at 24, 48, and 72 h postinjection of the PSs **4**, **12**, and **23** (at therapeutic dose 1 μmol/kg).

After whole-body imaging, the tumor was surgically removed from the original site (axilla) and placed on a shaved region of skin away from the original site as a means to image the skin flap (minus the tumor). Imaging was repeated as described before.

■ ASSOCIATED CONTENT

Ⓢ Supporting Information. ^{1}H and ^{13}C NMR spectra of all compounds; HPLC profiles of compounds **4**, **7**, **12**, and **23**; experimental details of known compounds; and spectroscopic data of compounds **10**, **18**, **21**, and **22**. This material is available free of charge via the Internet at http://pubs.acs.org.

■ AUTHOR INFORMATION

Corresponding Author

*R.K.P.: telephone, 716-845-3203; fax, 716-845-8920; e-mail, ravindra.pandey@roswellpark.org. H.B.: telephone, 716-845- 4587; fax, 716-845-5908; e-mail, heinz.baumann@roswellpark.org.

■ ACKNOWLEDGMENT

The help rendered by Paula Pera in animal studies is highly appreciated. The authors are thankful to NIH RO1CA127369, PO1 CA55791 (partial), and the shared resources of the Roswell Park Cancer Center support grant CA16056 for the financial assistance.

■ ABBREVIATIONS USED

PS, photosensitizer; PDT, photodynamic therapy; PET, positron emission tomography; STAT3, signal transducer and activation of transcription 3; ROI, region of interest; NMR, nuclear magnetic resonance; HRMS, high resolution mass spectrometry; FDG, fluorodeoxyglucose; SAR, structure−activity relationship

■ REFERENCES

(1) Schrevens, L.; Lorent, N.; Dooms, C.; Vensteenkiste, J. The role of PET scan in diagnosis, staging and management of non-small cell lung cancer. *The Oncologist* **2004**, *9*, 633–643.

(2) Evans, J. W.; Peters, A. M. Gamma camera imaging in malignancy. *Eur. J. Cancer* **2002**, *38*, 2157–2172.

(3) Gambhir, S. S. Molecular imaging of cancer with PET. *Nat. Rev. Cancer* **2002**, *2*, 683–693.

(4) Ametamey, S. M.; Honer; Schubiger, P. A. Molecular Imaging and PET. *Chem. Rev.* **2008**, *108*, 1501–1516.

(5) Jogoda, E.; Lang, L.; Caraco, C.; Neumann, R. D.; Sung, C.; Eckleman, W. C. Targeting of tranferrin receptors in nude mice bearing A431 and LS174T xenografts with[18F]holo-transferrin: permeability and receptor dependence. *J. Nucl. Med.* **1999**, *40*, 1547–1555.

(6) (a) Marom, E. M.; Erasmus, J. J.; Patz, E. F. Lung cancer and positron emission tomography with fluorodeoxyglucose. *Lung Cancer* **2000**, *28*, 187–202. (b) Taylor, M.; Wallhaus, T. R.; DeGrado, T. R.; Russell, D. C.; Stanko, P.; Nickles, R. J.; Stone, C. K. An evaluation of myocardial fatty acid and glucose uptake using PET with ^{18}F-FDG in patients with congestive heart failure. *J. Nucl. Med.* **2001**, *42*, 55–62. (c) Foster, N. L.; Heidebrink, J. L.; Claek, C. M.; Jagust, W. J.; Arnold, S. E.; Barbas, N. Y.; DeCarli, C. S.; Turner, R. S.; Koeppe, R. A.; Higdon, R.; Minoshima, S. FDG-PET improves accuracy in distinguishing frontotemporal dementia and Alzheimer's disease. *Brain* **2007**, *130*, 2616–2635.

(7) Cook, G. J.; Houston, S.; Rubens, R.; Maisey, M. N.; Fogelman, I. Detection of bone metastases in breast cancer by FDG: Differing metabolic activity in osteoblastic and osteolytic lesions. *J. Clin. Oncol.* **1998**, *16*, 3375–3379.

(8) Minoshima, S.; Frey, K. A.; Koeppe, R. A.; Foster, N. L.; Kuhl, D. E. A diagnostic approach in Alzheimer's disease using three dimentional stereotactic surface projections of fluorine-18-FDG. *J. Nucl. Med.* **1995**, *36*, 1238–1248.

(9) Von Schulthess, G. K. Molecular Anatomic Imaging (DVD); Schmid, D., Ed.; Lippincott Williams & Wilkins: 2007.

(10) Rajgopalan, R.; Grummon, G. D.; Bugaj, J.; Halleman, L. S.; Webb, E. G.; Marmion, M. E.; Vanderheyden, J. L.; Srinivasan, A. Preparation, characterization, and biological evaluation of Technetium-(V) and Rhenium(V) Complexes of Novel Heterocyclic Tetradentate N_3S Ligands. *Bioconjugate Chem.* **1997**, *8*, 407–415.

(11) (a) Chang, F.; Rusckowski, M.; Qu, T.; Hanatowich, D. J. Early results in the irrational design of new bifunctional chelators. *Cancer* **1997**, *80*, 2347–2353. (b) Volkert, W. A.; Hoffman, T. J. Therapeutic Radiopharmaceuticals. *Chem. Rev.* **1999**, *99*, 2269–2292.(c) Lamonica, D.; Grossman, Z.; Klippenstein, D.; Wang, H.; Vilani, J.: Nabi, H. A comparative study of 511 keV SPECT and PET using separate 370 MBq F-18-FDG doses on different days. *Clin. Positron Imaging* **1999**, *2*, 81−91.

(12) Pandey, R. K.; Goswami, L. N.; Chen, Y.; Gryshuk, A.; Missert, J. R.; Oseroff, A.; Dougherty, T. J. Nature: A rich source for developing multifunctional agents. Tumor-imaging and photodynamic therapy. *Lasers Surgery Med.* **2006**, *38*, 445–467.

(13) Ethirajan, M.; Patel, N. J.; Pandey, R. K. Porphyrin-based multifunctional agents for tumor-imaging and PDT. In *Handbook of Porphyrin Science*; Vol. 4, Phototherapy, Tadioimmunotherapy and Imaging; Kadish, K. M., Smith, K. M., Guilard, R., Eds.; World Scientific: 2010.

(14) Ethirajan, M.; Chen, Y.; Joshi, P.; Pandey, R. K. The role of porphyrin chemistry in tumor-imaging and photodynamic therapy. *Chem. Soc. Rev.* **2011**, *40*, 340–362.

(15) (a) Gomer, C. J., Ed. Photodynamic Therapy. *Methods in Molecular Biology*; Springer: New York, 2010. (b) Herman, C.; Pandey, R. K. Shedding some light on tumors. *Chem. Ind. (London)* **1998**, 739–743.

(16) Hasan, T.; Parish, J. A. *Photodynamic therapy of cancer in Cancer Medicine*, 4th ed.; Williams & Wilkins: Baltimore, MD, 1997; pp 739−750.

(17) Henderson, B. W.; Gollnick, S. O. Mechanistic Principles of Photodynamic Therapy. In *Organic Photochemistry and Photobiology*; Horspool, W., Lenci, F., Eds.; CRC Press: Boca Raton, FL, 2003.

(18) Olenick, N. L.; Morris, R. L.; Belichenko, I. The role of apoptosis in response to photodynamic therapy of cancer: What, where, why and how? *Photochem. Photobiol. Sci.* **2002**, *1*, 1–21and references therein.

(19) Osterloh, J.; Vicente, M. G. H. Mechanisms of Porphyrinoid llocalization in tumors. *J. Porphyrins Phthalocyanines* **2002**, *6*, 305–324.

(20) Sharman, W. M.; Allen, C. M.; Van Lier, J. E. Role of activated oxygen species in Photodynamic Therapy. *Methods Enzymol.* **2000**, *319*, 376–386.

(21) Pandey, R. K.; Sumlin, A. B.; Potter, W. R.; Bellnier, D. A.; Henderson, B. W.; Constanatine, S.; Aoudia, M.; Rodgers, M. A. J.; Smith, K. M.; Dougherty, T. J. Structure and Photodynamic Efficacy Among Alkyl Ether Analogs of Chlorophyll-*a* Derivatives. *Photochem. Photobiol.* **1996**, *63*, 194–205.

(22) Henderson, B. W.; Bellnier, D. A.; Graco, W. R.; Sharma, A.; Pandey, R. K.; Vaughan, L.; Weishaupt, K. R.; Dougherty, T. J. A quantitative structure activity relationship for a congeneric series of pyropheophorbide derivatives as photosensitizers for photodynamic therapy. *Cancer Res.* **1997**, *57*, 4000–4007.

(23) Dougherty, T. J.; Pandey, R. K.; Nava, H. R.; Smith, J. A.; Douglass, H. O.; Edge, S. B.; Bellnier, D. A.; O'Malley, L.; Cooper, M. Preliminary clinical data of a new photodynamic therapy photosensitizers, HPPH for treatment of obstructive esophageal cancer. *Proc. SPIE* **2000**, *3909*, 25–27.

(24) Bellnier, D. A.; Greco, W. R.; Loewen, G. M.; Nava, V.; Oseroff, A. R.; Pandey, R. K.; Tsuchida, T.; Dougherty, T. J. Population pharmacokinetics of the photodynamic therapy agent HPPH in cancer patients. *Cancer Res.* **2003**, *63*, 1806–1813.

(25) Ma, B.; Li, G.; Kanter, P.; Lamonica, D.; Grossman, Z.; Pandey, R. K. Bifunctional HPPH-N_2S_2-Tc-099m conjugates as tumor imaging agents: synthesis and biodistribution studies. *J. Porphyrins Phthalocyanines* **2003**, *7*, 500–507.

(26) Pandey, S. K.; Gryshuk, A. L.; Sajjad, M.; Zheng, X.; Chen, Y.; Abouzeid, M. M.; Maogan, J.; Charamisinau, I.; Nabi, H. A.; Pseroff, A.; Pandey, R. K. Multimodality agents for tumor-imaging (PET, Fluorescence) and Photodynamic Therapy: A possible "See and Treat" approach. *J. Med. Chem.* **2005**, *48*, 6286–6295.

(27) Pandey, S. K.; Sajjad, M.; Chen, Y.; Pandey, A.; Missert, J. R.; Batt, C.; Yao, R.; Nabi, H. A.; Pseroff, A. R.; Pandey, R. L. Compared to purpurinimides, the pyropheophorbide containing an iodobenzyl group showed enhanced PDT efficacy and tumor imaging ability. *Bioconjugate Chem.* **2009**, *20*, 274–282.

(28) Pandey, S. K.; Sajjad, M.; Chen, Y.; Zheng, X.; Yao, R.; Missert, J. R.; Batt, C.; Nabi, H. A.; Oseroff, A. R.; Pandey, R. K. Comparative positron-emission tomography (PET) imaging and phototherapeutic potential of ^{124}I-labeled methyl-3-(1′-iodobenzyloxyethyl) pyropheophorbide-*a* vs the corresponding glucoase- and galactose conjugates. *J. Med. Chem.* **2009**, *52*, 445–455.

(29) Chao, L.; Dobhal, M. P.; Ethirajan, M.; Missert, J. R.; Pandey, R. K.; Balasubramanian, S.; Sukumaran, D. K.; Zhang, M.; Kadish, K. M.; Ohkubo, K.; Fukuzumi, S. Highly selective synthesis of ring-B reduced chlorins by ferric chloride-mediated oxidation of bacteriochlorins: Effects of the fused imide vs isocyclic ring on photophysical and electrochemical properties. *J. Am. Chem. Soc.* **2008**, *130*, 14311–14323.

(30) Zheng, X.; Morgan, J.; Pandey, R. K.; Chen, Y.; Tracy, E.; Baumann, H.; Missert, J. R.; Batt, C.; Jackson, J.; Bellnier, D. A.; Henderson, B. W.; Pandey, R. K. Conjugation of HPPH to carbohydrates changes its subcellular distribution and enhances photodynamic activity in vivo. *J. Med. Chem.* **2009**, *52*, 4306–4318.

(31) (a) Henderson, B. W.; Daroqui, C.; Tracy, E.; Vaughan, L. A.; Loewen, G. M.; Cooper, M. T.; Baumann, H. Cross-linking of signal transducer and activator of transcription-3- A molecular marker for the photodynamic reaction in cells and tumors. *Clin. Cancer Res.* **2007**, *13*, 3156–3163. (b) Chen, Y.; Ohkubo, K.; Zhang, M.; Wenbo, E.; Liu, W.; Cieseelski, M.; Baumann, M.; Fukuzumi, S.; Kadish, K. M.; Fenstermaker, R.; Oseroff, A. R.; Pandey, R. K. Photophysical, electrochemical characteristics and cross linking STAT-3 protein by an efficient bifunctional agent for fluorescence image-guided photodynamic therapy. *Photochem. Photobiol. Sci.* **2007**, *12*, 1257–1267.